Received: 13 September 2024 | Revised: 25 January 2025 | Accepted: 27 January 2025

DOI: 10.1002/qj.4951

Quarterly Journal of the Royal Meteorological Society RMetS

RESEARCH ARTICLE

Seasonal and regional variation in drop size distributions for different types of rain over northeastern and eastern parts of India

Imolemba Longkumer[1,2] | **Rupraj Biswasharma**[2] | **Imlisunup Pongener**[1] | **Debajyoti Samanta**[3] | **Mahen Konwar**[2] | **Sanjay Sharma**[4]

[1]Department of Physics, Kohima Science College, Kohima, Nagaland, India

[2]Indian Institute of Tropical Meteorology, Ministry of Earth Sciences, Pune, Maharashtra, India

[3]Department of Physics, Rampurhat College, Rampurhat, West Bengal, India

[4]Department of Higher Education, Dimapur Government College, Dimapur, Nagaland, India

Correspondence
Sanjay Sharma, Dimapur Government College, Dimapur, Nagaland, 797112, India.
Email: sanjay_sharma11@hotmail.com

Funding information
Ministry of Education, India; Council of Scientific and Industrial Research, India; Science and Engineering Research Board, Grant/Award Number: PDF/2022/002060; Ministry of Education, Govt. of India, and the Govt. of Nagaland,

Abstract

Seasonal and regional variations of Drop Size Distributions (DSDs) of rain are studied at Kohima (25.67° N, 94.08° E) in northeastern India and Rampurhat (24.17° N, 87.78° E) in eastern India, using six years (2017–2022) of data from the OTT Parsivel^2 disdrometer. The DSDs are quantified with gamma distributions and analyzed based on parameters such as slope (Λ, mm^{-1}), shape (μ), normalized intercept parameter (N_w, mm$^{-1}\cdot$m^{-3}), mass-weighted mean diameter (D_m, mm) and radar reflectivity factor (Z, dBZ). Seasonally, larger raindrops prevail during the pre-monsoon and smaller ones during the monsoon at both stations. Regionally Rampurhat exhibits larger drops compared to Kohima. In both seasons and stations, larger raindrops are found for convective rain than stratiform rain. The observed seasonal and regional variations of surface D_m align with Global Precipitation Measurement (GPM) onboard Dual-frequency Precipitation Radar (DPR) observations. Distinct clusters of D_m–$\log_{10}N_w$ suggest maritime characteristics at Kohima and continental characteristics at Rampurhat. Power law relationships are found for N_w–R, D_m–R and Z–R. Exponent values of Z–R relationships indicate that microphysical processes are mainly driven by both breakup and collision–coalescence (number and size-controlled) processes. Extremely large-size raindrops (~8 mm) and intense rainfall ($R > 150$ mm$\cdot$hr^{-1}) are noted during convective rain at Rampurhat.

KEYWORDS

disdrometer, rain microphysics, raindrop size distribution, stratiform rain, convective rain

1 | INTRODUCTION

Understanding of rain's Drop Size Distributions (DSDs) in different geographical locations is important as it has a regional and seasonal variability and has wide applications in the remote measurement of rain, design of radio communication links, modeling of soil erosion and parameterization of the rain microphysical process of precipitation systems in Numerical Weather Prediction (NWP) models. The natural variation of rain's DSDs lead to non-unique radar reflectivity factor (Z)–rainfall intensity (R) relationships, which pose a greater challenge to find an optimum relation for quantitative precipitation estimation. Observing DSDs across diverse locations can

   Q J R Meteorol Soc. 2025;151:e4951. https://doi.org/10.1002/qj.4951

help minimize the knowledge gap on the microphysical properties of rain. Therefore, studying DSD variability across locations with significantly different topographical and climatic conditions is essential. In this study, based on six years (2017–2022) of long-term observations made using OTT particle velocity (Parsivel^2) disdrometers, we report on the DSD variability between two locations: Rampurhat, West Bengal, India, situated in the plain valley near the Bay of Bengal, and Kohima, Nagaland, India, located in the hilly terrain of northeast India.

Aspects of seasonal, regional, and diurnal variations of DSDs have been reported from different locations across the globe. For example, Kozu et al. (2006) studied seasonal and diurnal variations of rain DSDs in the Asian monsoon region at different stations (Gadanki [India], Singapore and Kototabang [Indonesia]). They reported that DSDs at Gadanki have significant seasonal variation, whereas DSDs at Kototabang have significant diurnal variation, while Singapore has less diurnal and seasonal variations. Over India, Radhakrishna et al. (2009) reported distinct spatial and seasonal DSD characteristics during the southwest and northeast monsoon seasons between an inland station, Gadanki, and a coastal station, Cuddalore. The study of rain microphysical properties over the northeastern and eastern parts of India is limited, with only a few recent reports, such as those by Murata et al. (2020) and Longkumer et al. (2023). Due to the lack of long-term continuous DSD observations, the seasonal variations in DSD between the hilly terrain of northeast India and the plain valleys near the Bay of Bengal remain largely unknown. Differences in DSD parameters between these two contrasting regions are, however, naturally expected due to variations in topography, wind patterns, large-scale circulation, and local convection. Understanding such regional variability is crucial, as rain parameters are highly variable.

Using long-term measurements of DSDs, many studies have reported regional variations of DSD. In-situ DSD measurements and storm structures over the Western Ghats indicate that rainfall occur mostly from shallow clouds, which are characterized by small-size raindrops (Das et al., 2017; Konwar et al., 2014). Over Colorado, raindrops at a foothill station were observed to be smaller in size than those at a plain station (Friedrich et al., 2016). Seela et al. (2017) reported diverse rain DSDs in Palau and Taiwan, with relatively larger-size raindrops at Taiwan stations. In southern China at Zhuhai, Zhang et al. (2019) reported higher occurrences of smaller drops compared to eastern and northern China as reported by Chen et al. (2013) and Wen et al. (2017), respectively. At an inland station in Malaysia, Johor, a relatively higher concentration of large-size raindrops was observed compared to Gan and Manus Island in the Indian Ocean and Pacific Ocean, respectively (Alhilali et al., 2018). A systematic variation of DSD characteristics and corresponding Z–R relationships during convective and stratiform rain at inland and coastal stations in South Korea was reported by Suh et al. (2021). The difference in DSDs between the central and southern regions of South Korea was highlighted by Loh et al. (2019).

The continental and maritime characteristics of DSDs can be evaluated from two DSD parameters, namely, N_w and D_m, where N_w is the generalized intercept parameter of normalized gamma DSD and D_m is the mass-weighted mean diameter (Bringi et al., 2003; Tenorio et al., 2012). The continental nature is found to be associated with larger D_m and smaller N_w, whereas the maritime nature is found to be associated with smaller D_m and larger N_w. The regional variability of rain's DSDs observed along the equator in Indonesia using a network of disdrometers shows maritime-like DSD and the influence of both oceanic and continental systems over the four stations (Marzuki et al., 2013). During the Meiyu season in China, Chen et al. (2013) reported distinct rain DSD characteristics at Nanjing compared to other stations. Inland convective clouds along the leeward side of the Western Ghats (WGs) indicate a composite of maritime and continental characteristics (Konwar et al., 2022). The DSD of WGs bears a signature of maritime characteristics (Krishna et al., 2021). According to Lavanya and Kirankumar (2021), the DSD parameters observed at Thumba, a coastal station in Kerala, indicate that pre-monsoonal rainfall primarily originates from continental sources, and monsoonal rainfall is predominantly maritime in nature, while post-monsoonal rainfall reflects a combination of both maritime and continental influences. Shaik et al. (2024) reported regional and seasonal variation of rain DSDs at Kolkata, an inland station in eastern Peninsular India and Trivandrum, a coastal station in southern India. Their results were found to be consistent with the continental and maritime characteristics of rain DSDs. This study throws some light on the continental and maritime properties of DSD over Kohima and Rampurhat.

A pertinent question arises, what is the comparison between the in-situ measured and satellite measured DSD parameter? For example, in the data of the Global Precipitation Measurement (GPM) satellite, equipped with an onboard Ku (13.6 GHz) and Ka (35.5 GHz) Dual-Frequency Precipitation Radar (DPR), which estimates DSD parameters, i.e., D_m and N_w. Many studies have analyzed the estimated D_m from GPM-DPR and reported on rain properties. For example, Seto et al. (2016) reported larger (smaller) D_m values over land (ocean). The results also show seasonal variation of D_m over India, showing larger values from February to May and from September to November and smaller values in July and December. Similarly, Yamaji et al. (2020) also highlighted larger D_m

values over the land than the oceans for deep-cloud systems. The result also shows seasonal variation of D_m over the northwest Pacific Ocean, where variation is attributed to the change in the dominant precipitation systems. Over the mid-latitude and subtropical regions, the D_m shows larger values during winter and summer, attributing them to extratropical frontal systems and tropical disturbances, respectively. During the Indian summer monsoon Kumar and Silva (2019) studied the vertical characteristics of Z and DSD parameters for intense convective clouds, where the result shows a large hydrometeor size and lower concentrations for intense Z profiles. The result also shows a larger (smaller) hydrometeor size over the Western Himalaya foothills (Bay of Bengal). Over the land and topographic areas, the size of hydrometeors was larger whereas over oceanic areas the concentrations of hydrometeors were higher. A similar result is also reported by Radhakrishna et al. (2020) for deep systems showing larger D_m values for continental rain as compared to maritime and orographic rain. They also reported that northwest India and southeast Peninsular India (Western Ghats, Myanmar Coast and Arabian Sea) exhibit large (small) D_m values. They further reported that for shallow systems, the D_m values are smaller for continental rain compared to maritime and orographic rain, while northwest India and southeast Peninsular India (Bay of Bengal and Arabian Sea) show the smallest (largest) D_m values. The present study focuses on comparing D_m values as measured by the GPM satellite with surface observations.

The manuscript aims to address the following scientific objectives:

- To understand the regional and seasonal variations in rain DSDs between a hilly station in northeastern India and a plain region in eastern India.
- To determine the continental and maritime characteristics of rain DSD.
- To understand cloud microphysical properties and dynamical properties of the atmosphere of these two locations.

The manuscript is organized as follows. Section 2 provides details about the study region; Section 3 describes observational systems and methodology. The results of the study are discussed in Section 4. Section 5 consists of a discussion and summary and Section 6 provides the conclusion.

2 | STUDY REGION AND OBSERVATION STATIONS

The present study regions, i.e., Rampurhat (24.17° N, 87.78° E, 40 m above mean sea level (amsl), located in the Chotanagpur plateau of eastern India and Kohima (25.67° N, 94.08° E, 1500 m amsl) located in the Patkai hill range of northeast India, are shown in Figure 1. We also show the mean wind at 850 mb pressure level obtained from the European Centre for Medium-Range Weather Forecasts (ECMWF) Reanalysis dataset version 5.0 (ERA-5) (Hersbach et al., 2018). The eastern region of India is one of the most active convective zones in the globe, where fatality rate due to lightning strikes is significantly high (Illiyas et al., 2014). Frequent deep convective systems occur over this region during the pre-monsoon and monsoon seasons (Bhatt & Nakamura, 2005, 2006; Choudhury et al., 2015; Houze et al., 2007; Romatschke et al., 2010; Romatschke & Houze, 2011; Romatschke & Houze Jr., 2011; Roy et al., 2017, 2023; Zipser et al., 2006). During the pre-monsoon, interactions of different air masses (warm, moist southerly vs cool, dry westerly) and strong land heating over the Chotanagpur Plateau provide favorable synoptic conditions for the genesis of Nor'westers (Litta et al., 2012; Yamane & Hayashi, 2006),

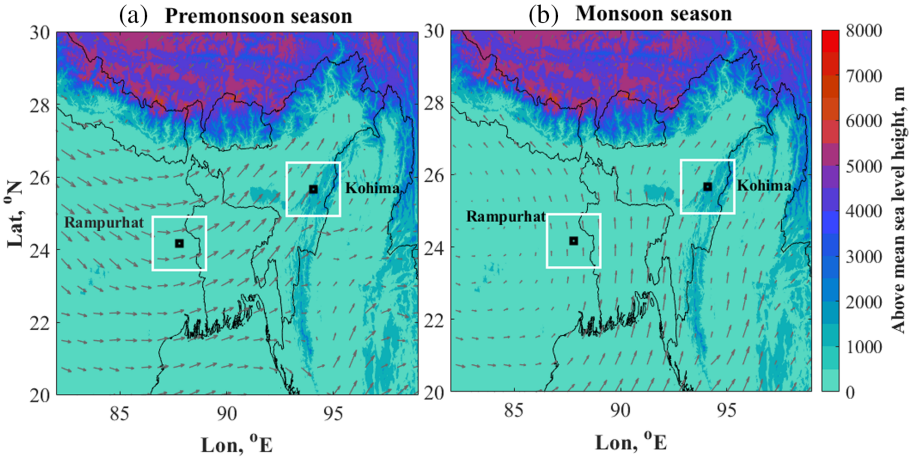

FIGURE 1 Study region with ground observatory at Rampurhat (24.17° N, 87.78° E) and Kohima (25.67° N, 94.08° E) during the (a) pre-monsoon and (b) monsoon seasons. The small black squares indicate both locations, while the large-size (white) boxes indicate the area considered for analysis of ERA-5 reanalysis data. Mean wind at 850 m is also shown on the respective panels. Color shading represents the topographical features. [Colour figure can be viewed at wileyonlinelibrary.com]

whereas during the monsoon the influence of the southwesterly monsoon winds, low-pressure systems, and monsoon depressions originating in the Bay of Bengal produces widespread, sustained, and often heavy rainfall.

The rain events over the northeastern region are generally associated with mesoscale structures of convection, which are embedded in much larger-scale convective organization (Choudhury et al., 2015; Goswami et al., 2010). They showed that the interaction of mesoscale circulation with the local topography generates southward-propagating gravity waves and associated strong updrafts, culminating to deep convective systems and extreme rainfall. The region of the eastern Himalaya foothills in the northeast consists of relatively weak Mesoscale Convective Systems (MCSs) with marginal changes in their intensity from pre-monsoon to monsoon.

The two regions, Kohima and Rampurhat, have distinctly different cloud microphysical and thermodynamical and electrical properties of precipitating systems (Biswasharma et al., 2021; Choudhury et al., 2015; Roy et al., 2017, 2020; Roy et al., 2023). Given the differences in topography, meteorological, thermodynamic and precipitating systems between these two locations, a study highlighting the regional and seasonal difference in DSD properties for different types of rain has been carried out in a comprehensive and integrated manner. To the best of our knowledge, the present study is the first of its kind over these regions.

3 | OBSERVATIONAL SYSTEMS AND DATA PRODUCTS

3.1 | OTT Parsivel^2 Disdrometer

OTT Parsivel^2 Disdrometer (OPD) is a second-generation laser-based optical disdrometer manufactured by OTT Hydromet, Germany. It is designed for both counting and measuring the size and fall speed of all types of precipitating particles. The working principle of OPD has been discussed extensively (Battaglia et al., 2010; Friedrich et al., 2013; Friedrich & Kalina, 2013; Jaffrain & Berne, 2011; Löffler-Mang & Joss, 2000; Raupach & Berne, 2015; Tokay et al., 2014; Yuter et al., 2006). The OPD has an optical sensor which produces a horizontal rectangular sheet of light having dimensions of $180 \times 30\,mm^2$ with a thickness of 1 mm. The laser beam is produced by a 650-nm laser diode with an output power of 3 mW. When the precipitating particles fall on the light sheet, there is a decrease in the signal resulting in a reduced voltage at the receiver, where the amplitude of the signal deviation is a measure of the particle size, and the duration of the signal allows an estimate of the particle fall velocity. It can measure the particle size and fall velocity within the range of 0.2–25 mm and 0.2–20 ms^{-1}, respectively. The measured particles are stored in size diameter and fall velocity bins in a 32×2 matrix corresponding to 32 non-equidistant classes of diameter and 32 non-equidistant classes of fall speed. The first two lower classes of diameter are kept empty always because of their low signal-to-noise ratio (Battaglia et al., 2010; Jaffrain & Berne, 2011; Niu et al., 2010; Tokay et al., 2013). Battaglia et al. (2010) described in detail the retrieval rationale of the OPD. The measurement of particle diameter by the OPD is done by following the spheroid model derived from Andsager et al. (1999) to estimate particle size as a function of voltage reduction. Particle sizes with diameter $D < 1$ are assumed to be spherical (axis of rotation = 1), for particles with D between 1 and 5 mm, the assumed axis ratio varies from 1 to 1.3 linearly and for particles with $D > 5$ mm, the axis ratio is taken as 1.3 (Yuter et al., 2006). Löffler-Mang and Joss (2000) compared the DSD observations from OPD with the Joss–Waldvogel disdrometer and found that the error in determining size in the whole range did not exceed $\pm 100\,\mu m$. For the measurement of fall velocity, the error is larger, around 25% for the smallest drops (0.3 mm) and decreasing to 10% for the largest drops (5 mm). Like any other instrument, OPD also suffers some instrument errors such as quantization error, marginal effect error, splashing effect error, insensitivity to smaller drops error, and multiple drop occurrence error as discussed in many articles (Battaglia et al., 2010; Jaffrain & Berne, 2011; Janapati et al., 2017; Krajewski et al., 2006; Löffler-Mang & Joss, 2000; Niu et al., 2010; Yuter et al., 2006). The specification of the details of the OPD is provided in Table S1. The present study is carried out by analyzing six years (2017–2022) of observations at Kohima and Rampurhat. The time resolution for the present study is 1 min.

The rain drop number density $N(D_i)$ is calculated by using the following equation

$$N(D_i) = \sum_{j=1}^{32} \frac{n_{ij}}{S_{\text{eff}}.\Delta t.V_j.\Delta D_i}, \tag{3}$$

where D_i is the mean of the ith diameter class, n_{ij} is the number of drop within the ith size and velocity bin j. $S_{\text{eff}}(D_i)$ is the effective sampling area $L\left(W - \frac{D_i}{2}\right)$. L is the length of the laser beam (180 mm), W is width of the laser beam (30 mm), and Δt is the sampling time, V_j (m/s) is the fall speed for the jth velocity bin. ΔD_i is the ith diameter interval (mm).

The nth moment of rain DSDs is expressed as follows:

$$M_n = \sum_{i=1}^{32} N(D_i) D_i^n \Delta D_i. \tag{4}$$

From the moment equations (4), various rain integral parameters such as rain rate R (mm·hr^{-1}), rain liquid water content W (g·m^{-3}) and radar reflectivity factor Z (mm^6·m^{-3}) are calculated by using $N(D_i)$, i.e.:

$$R = \frac{6\pi}{10^4}\sum_{i=1}^{32}\sum_{j=1}^{32} V_j N(D_i) D_i^3 \Delta D_i, \tag{5}$$

$$W = \frac{\pi \rho_w}{6000}\sum_{i=1}^{32} N(D_i) D_i^3 \Delta D_i, \tag{6}$$

where the density of water (ρ_w) = 1.0 g·cm^{-3}.

$$Z = \sum_{i=1}^{32} N(D_i) D_i^6 \Delta D_i. \tag{7}$$

The normalized gamma DSD parameters are used to characterize microphysical properties of rain (Bringi et al., 2003; Sekhon & Srivastava, 1971; Testud et al., 2001; Willis, 1984). The normalized gamma DSD is of the following form:

$$N(D) = N_w f(\mu)\left(\frac{D}{D_m}\right)^{\mu} \exp\left[-(4+\mu)\frac{D}{D_m}\right], \tag{8}$$

where

$$f(\mu) = \frac{6}{4^4}\frac{(4+\mu)^{\mu+4}}{\Gamma(\mu+4)}. \tag{9}$$

μ is a measure of the shape of the gamma DSD (Bringi et al., 2003; Ulbrich, 1983; Ulbrich & Atlas, 1984). D (mm) is the raindrop diameter. D_m (mm) is the mass-weighted mean diameter and N_w (mm^{-3}·mm^{-1}) is the normalized intercept parameter.

Further, D_m (mm) and N_w (mm^{-1}·m^{-3}) can be calculated from the following equations (Bringi et al., 2003; Testud et al., 2001):

$$D_m = \frac{M_4}{M_3} = \frac{\sum_{i=1}^{32} D_i^4 N(D_i)\Delta D_i}{\sum_{i=1}^{32} D_i^3 N(D_i)\Delta D_i}; \tag{10}$$

$$N_w = \frac{4^4}{\pi \rho_w}\left(\frac{10^3 W}{D_m^4}\right) = \frac{128(M_3)^5}{3(M_4)^4}; \tag{11}$$

$$\mu = \frac{(7-11\eta) - \left(\eta^2 + 14\eta + 1\right)^{0.5}}{2(\eta - 1)}; \tag{12}$$

$$\Lambda = \left[\frac{M_2}{M_4}(\mu+3)(\mu+4)\right]^{0.5}; \tag{13}$$

where

$$\eta = \frac{M_4^2}{M_2 M_6}. \tag{14}$$

3.2 | Comparison of OPD with a tipping bucket rain gauge

Prior to using OPD data, validation of the instrument was carried out using simultaneous measurements from an Automatic Rain Gauge (ARG). Thirty minutes of rainfall accumulation from these two systems were compared for both Kohima (14,820 rainy minutes) and Rampurhat (5670 rainy minutes), as shown in Figure 2. These measurements show a good correlation of 0.97 and 0.90 over Kohima and Rampurhat, respectively. The OPD shows a slight underestimation compared to the rain gauge with biases of −0.26 mm and −0.63 mm over Kohima and Rampurhat, respectively. This underestimation is accompanied by increased scattering at higher rain accumulation at both stations, indicating a larger measurement error under such conditions. Overall, the performance of the two instruments shows a better fit over Kohima with an RMSE value of 0.35 mm compared to 0.98 mm at Rampurhat. Similar

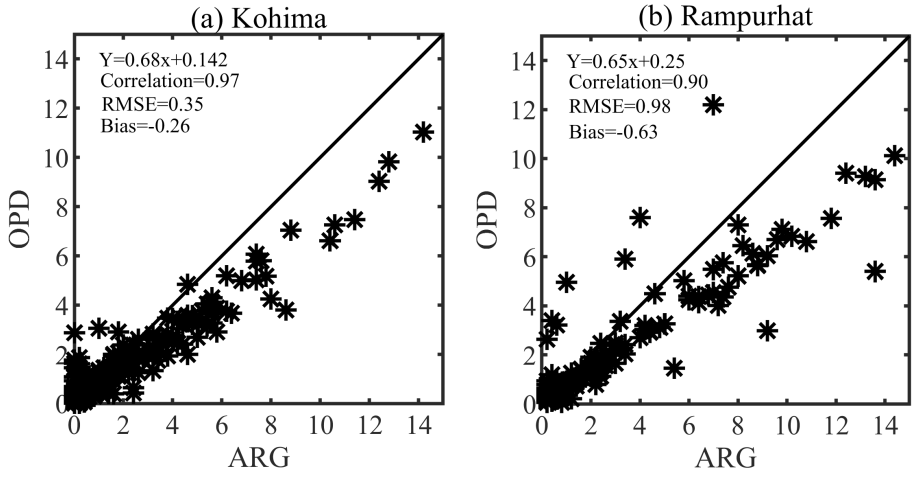

FIGURE 2 Scatter plots of 30-min rain accumulation measured by OPD and ARG over (a) Kohima and (b) Rampurhat.

results were also reported at Cherrapunji in northeastern India by Murata et al. (2020), where the OPD showed underestimation compared to the rain gauge.

3.3 | Classification of rain types using OPD observations

The classification of different rain types using a disdrometer has been done by many researchers using different methods. Classification of stratiform and convective rain types was shown by Bringi et al. (2003); Chen et al. (2013); Marzano et al. (2010); Testud et al. (2001); Tokay and Short (1996); Wang et al. (2020); and Zhang et al. (2019). Further, the classification of rain into three types, convective, stratiform and either stratocumulus or mixed type of rain, was also reported by Xie et al. (2020) and Zeng et al. (2020). For this study we considered only raindrops having a diameter ranging from 0.25 to 8 mm. An event is considered rainy if there is continuous rain of $R > 0.5\,\mathrm{mm{\cdot}h^{-1}}$ for at least 10 min. To get a better understanding of the characteristics of rain DSDs for different precipitation types, we classified the rain into three types, i.e., stratiform, mixed and convective rain by following Bringi et al. (2003) and Marzano et al. (2010). For any rainfall event, if at any instantaneous moment t_n, R is $\leq 5\,\mathrm{mm{\cdot}hr^{-1}}$ within the time range $[t_n - N_s,\ t_n + N_s]$, and the standard deviation is $\leq 1.5\,\mathrm{mm{\cdot}hr^{-1}}$, the event is classified as a stratiform event. If R is $>5\,\mathrm{mm{\cdot}hr^{-1}}$ and the standard deviation is $>1.5\,\mathrm{mm{\cdot}hr^{-1}}$ within the time range $[t_n - N_s,\ t_n + N_s]$, the event is classified as a convective rainfall event and those events which are neither stratiform nor convective are considered as mixed rainfall events. The N_s value is set to five samples in this study.

3.4 | GPM-DPR

The Global Precipitation Measurement (GPM) mission, launched on February 27, 2014, from Japan's Tanegashima Space Center, advances precipitation measurement through the Dual Precipitation Radar (DPR) and Microwave Imager (GMI). The DPR includes Ku-band (13.6 GHz) and Ka-band (35.5 GHz) channels, offering high-resolution precipitation profiling. As the second spaceborne precipitation radar following Tropical Rainfall Measuring Mission (TRMM's) Precipitation Radar, the DPR provides Level-2A data (2A-DPR, version 07A) with an ~5 km nadir footprint. This study utilizes the DSD parameter, namely mass-weighted mean diameter (D_m) obtained from the lowest clutter-free bin of the GPM-DPR 2A-DPR data to compare with the OPD observation, which is crucial for understanding rainfall microphysics (Iguchi et al., 2010). A total of 249 and 355 overpasses of DPR during 2017–2022 over Rampurhat and Kohima were considered. These overpasses were selected within a $2° \times 2°$ box centered over each region (Kohima and Rampurhat). The GPM products (2A-DPR) were obtained from the NASA/Goddard Space Flight Center's science team and PPS (https://storm.pps.eosdis.nasa.gov/storm/).

3.5 | Moderate resolution imaging spectroradiometer (MODIS)

MODIS, an Earth-observing sensor onboard the Terra and Aqua satellites, captures atmospheric and surface properties with global coverage every 1–2 days. Terra follows a morning equatorial crossing (north-to-south), while Aqua crosses in the afternoon (south-to-north). The primary focus of this study is on the cloud Liquid Effective Radius (LER) derived from MODIS-Aqua data. LER characterizes the size of liquid water droplets in clouds, a critical parameter in understanding cloud microphysics and radiative properties. The MODIS-Aqua dataset (2017–2022) was employed to examine seasonal and regional variations in cloud LER, providing insights into cloud properties and their role in atmospheric processes.

3.6 | ERA-5 reanalysis data

The ERA-5 reanalysis dataset offers high-resolution insights into atmospheric dynamics with hourly data at a $0.25° \times 0.25°$ resolution across 37 vertical pressure levels (1000–1 hPa). It integrates observations from satellites, weather stations, and balloons with NWP models, generating vertical air motion data (omega, ω). Omega represents upward (negative) or downward (positive) air motion, essential for understanding convective dynamics, storm development, and monsoonal processes, to understand the dynamical properties of the atmosphere. The vertical wind during the pre-monsoon and monsoon seasons is studied by using fifth-generation ERA-5 datasets (Hersbach et al., 2018). ERA-5 calculates vertical pressure velocity or omega which is estimated from the horizontal divergence equation of wind (Tanaka & Yatagai, 2000).

Although we utilized reanalysis datasets, we ensured their reliability by validating the ERA-5 total precipitation data against surface rainfall observations from rain gauges. To assess this, we compared the daily accumulated surface rainfall in 2018 over the two study regions. Scatter plots, provided in Figure S1, demonstrate a reasonably good correlation of 0.55 for Kohima and 0.42 for Rampurhat. This establishes the ERA-5 dataset as sufficiently reliable for the

relevant areas, supporting its use in subsequent analyses within this study.

For consistency and comparability across datasets, a $2 \times 2°$ spatial region around the ground observatory was selected for all the platforms beside the ground observations. This facilitates an integrated analysis of precipitation microphysics, cloud properties, and atmospheric dynamics using GPM-DPR, MODIS, and ERA-5 data. Matching ground-based observations with satellites and reanalysis data point-by-point in space and time is challenging due to their differing original purposes and spatial–temporal resolutions. Our overall broad goal, however, is to identify qualitative and statistical patterns across these multiplatform datasets. This approach enables a comprehensive intercomparison, enhancing the reliability and validity of the obtained results while bridging the gap between localized measurements and broader-scale analyses.

4 | RESULTS

4.1 | Rain DSD characteristics

The seasonal and regional variations of the average *N(D)* for stratiform, mixed and convective rain are shown in Figure 3a–c respectively. The number of spectra averaged and average *R* for each case are provided in Table 1. The corresponding properties of D_m, $log_{10}N_w$, Λ and μ for stratiform, mixed and convective types of rain at both stations during pre-monsoon and monsoon are shown by the box plots in Figure 4. The Q_2 (50th percentile), Q_3 (75th percentile), UW (Upper Whisker) values of D_m, $\log_{10}N_w$, Λ and μ parameters are provided in Table 2. Details of seasonal and regional characteristics of DSDs are discussed in the following sections.

4.1.1 | Regional variability of DSDs

The mean DSD spectra (Figure 3) over Rampurhat distinctly shows higher concentration of larger drops ($D > 2$ mm) as compared to Kohima for all rain types both during pre-monsoon and monsoon season. Whereas the concentration of smaller drops ($D < 1$ mm) is significantly higher over Kohima. The presence of giant raindrops ($D \sim 8$ mm) in mixed and convective rains at Rampurhat during the pre-monsoon and monsoon seasons is noteworthy. This phenomenon could be attributed to intense convective activities over Rampurhat during these seasons. The existence of raindrops larger than 8 mm

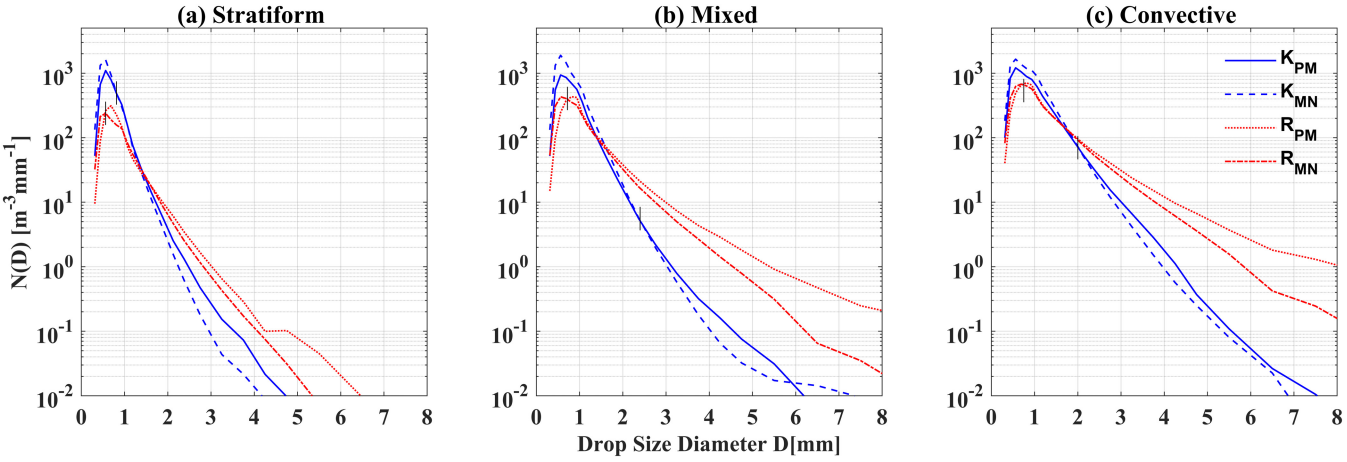

FIGURE 3 An *N(D)* versus *D* plot during the pre-monsoon and monsoon seasons over Kohima (blue) and Rampurhat (red) for (a) stratiform, (b) mixed and (c) convective types of rain (K_{PM}, Kohima pre-monsoon; K_{MN}, Kohima monsoon; R_{PM}, Rampurhat pre-monsoon; and R_{MN}, Rampurhat monsoon). The black vertical bar indicates the drop intercept (D_I). [Colour figure can be viewed at wileyonlinelibrary.com]

TABLE 1 Number of utilized rain DSD spectra and average *R*.

	Number of utilized DSD spectra (average *R*, mm·hr^{-1})					
	Premonsoon			Monsoon		
Station	Stratiform	Mixed	Convective	Stratiform	Mixed	Convective
Kohima	2912 (1.5)	3903 (4.1)	565 (17.3)	12,763 (1.5)	16,140 (5.7)	1566 (16.4)
Rampurhat	1030 (1.6)	2212 (11.0)	1232 (38.6)	4864 (1.6)	9650 (11.2)	3447 (38.8)

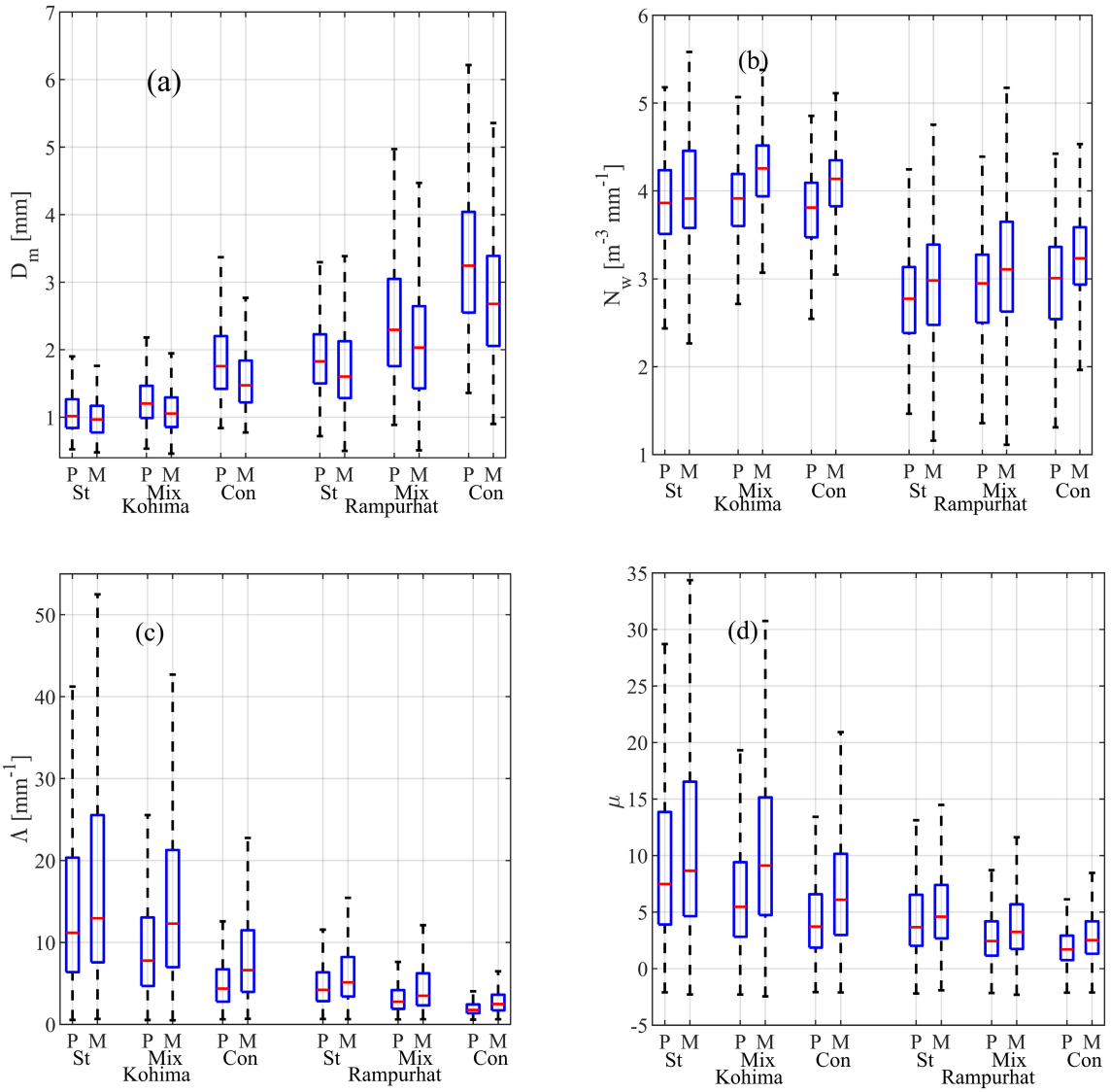

FIGURE 4 Box plots of surface D_m, log-normalized parameter $\log_{10}N_w$, slope parameter Λ, and shape parameter μ of the gamma model for stratiform (St), mixed (Mix) and convective (Con) types of rain over Kohima and Rampurhat during the pre-monsoon (P) and monsoon (M) seasons. [Colour figure can be viewed at wileyonlinelibrary.com]

($D > 8$ mm) appears plausible, but further investigation and measurements using precise instruments are required. Extremely large raindrops have been documented in other regions; for example, raindrops of $D \sim 8.8$ mm have been observed beneath cumulus congestus clouds in Brazil (Hobbs & Rangno, 2004). Gatlin et al. (2015) also reported giant raindrops ($D > 8$ mm) in tropical, subtropical, and high-latitude continental regions, with the largest raindrops, measuring $D \sim 9.7$ mm, observed in subtropical locations.

The Q_2, Q_3 and UW values from Table 2 and Figure 4 all show consistently larger (smaller) values of D_m ($log_{10}N_w$, Λ and μ) over Rampurhat compared to Kohima for all rain types during both the pre-monsoon and monsoon seasons. The results indicate broader DSDs with larger drops and lower concentrations of smaller drops over Rampurhat compared to Kohima. It is also found that the value of μ is positive at both the stations for all rain types, indicating concave downward DSD shape. The regional variability of rain DSDs during both the seasons shows the prevalence of a higher concentration of larger drops at Rampurhat.

4.1.2 | Seasonal variability of DSDs

To understand the seasonal characteristics of rain DSDs, the drop intercept D_I is determined. D_I is the diameter where two DSDs intersect. Over Kohima the D_I values between pre-monsoon and monsoon indicate 0.81, 2.40 and 2.00 mm for stratiform, mixed and convective

TABLE 2 D_m, $\log_{10}N_w$, Λ and μ values for different types of rain at Kohima and Rampurhat during the pre-monsoon and monsoon seasonS as observed from OPD. Q_2 indicates 50th percentile, Q_3 indicates 75th percentile and UW indicates the upper whisker of different DSD parameters. The values during the monsoon are indicated within parentheses.

		Kohima premonsoon (monsoon)			Rampuhat premonsoon (monsoon)		
		Q_2	Q_3	UW	Q_2	Q_3	UW
D_m	Stratiform	1.02 (0.97)	1.27 (1.17)	1.90 (1.76)	1.83 (1.60)	2.23 (2.13)	3.30 (3.39)
	Mixed	1.20 (1.06)	1.47 (1.29)	2.18 (1.95)	2.30 (2.03)	3.06 (2.65)	4.95 (4.48)
	Convective	1.76 (1.47)	2.20 (1.84)	3.37 (2.77)	3.28 (2.68)	4.24 (3.42)	6.75 (5.41)
$\log_{10}N_w$	Stratiform	3.86 (3.91)	4.24 (4.46)	5.18 (5.58)	2.77 (2.98)	3.13 (3.39)	4.24 (4.76)
	Mixed	3.92 (4.26)	4.20 (4.52)	5.07 (5.38)	2.93 (3.10)	3.27 (3.65)	4.39 (5.18)
	Convective	3.81 (4.14)	4.09 (4.35)	4.86 (5.11)	2.96 (3.22)	3.33 (3.58)	4.42 (4.53)
Λ	Stratiform	11 (13)	20 (26)	41 (53)	4 (5)	6 (8)	12 (15)
	Mixed	8 (12)	13 (21)	26 (43)	3 (4)	4 (6)	8 (12)
	Convective	4 (7)	8 (12)	13 (23)	2 (3)	3 (4)	4 (7)
μ	Stratiform	7 (9)	14 (17)	29 (34)	4 (5)	7 (7)	13 (15)
	Mixed	6 (9)	9 (15)	19 (31)	2 (3)	4 (6)	9 (12)
	Convective	4 (6)	7 (10)	13 (21)	2 (3)	3 (4)	6 (9)

Abbreviations: Q_2, 50th percentile; Q_3, 75th percentile; UW, upper whisker.

rain (Figure 3). Pre-monsoon rain shows a higher concentration of larger drops ($D > D_I$), while monsoon rain shows a higher concentration of smaller drops ($D < D_I$). This indicates a dominance of larger drops during the pre-monsoon and smaller drops during the monsoon seasons. The peak of *N(D)* over Kohima is 0.56 mm for all rain types in both the seasons. As the season progresses, a significant increase in the concentration around the peak D is observed for all rain types. It is interesting to note that though R remains comparable during the pre-monsoon and monsoon seasons (Table 1), the DSD characteristics underwent substantial changes. Seasonally, at Kohima, as shown in Figure 4 for all rain types, the Q_2, Q_3 and UW show larger D_m and smaller $\log_{10}N_w$, Λ and μ values during the pre-monsoon season. This indicates a higher concentration of larger drops with broader DSDs and fewer smaller drops. Thus, distinct seasonal DSD characteristics are observed for different rain types over Kohima.

At Rampurhat, peak *N(D)* occurred at diameters of approximately $D \sim 0.69$ mm, 0.81 mm and 0.81 mm during the pre-monsoon season, and 0.56 mm, 0.56 mm and 0.69 mm during the monsoon season for stratiform, mixed and convective rain, respectively. Unlike Kohima, there is a shift in the peak D, which moves toward smaller drops from the pre-monsoon to the monsoon season. The D_I values for pre-monsoon and monsoon seasons are 0.56 mm, 0.72 mm and 0.75 mm for stratiform, mixed and convective rain, respectively. Pre-monsoon rain shows a higher concentration of larger drops ($D > D_I$), while monsoon rain a shows higher concentration of smaller drops ($D < D_I$). This indicates a dominance of larger drops during the pre-monsoon season and smaller drops during the monsoon season. Similarly, the Q_2, Q_3 and UW also show larger D_m and smaller $\log_{10}N_w$, Λ and μ during the pre-monsoon season, indicating a higher concentration of larger drops with broader DSDs along the larger drops and fewer smaller drop compared to the monsoon season, as shown in Figure 4.

In terms of rain types at both stations during both seasons, the convective rain consistently shows larger (smaller) values of D_m (Λ and μ) compared to the stratiform and mixed rain, suggesting broader DSDs among larger drops. The DSD characteristics of mixed types of rain lie between stratiform and convective rain in all cases. Over Kohima, the stratiform rain shows a larger value of $\log_{10}N_w$ suggesting a higher concentrations of smaller drops, whereas at Rampurhat a higher concentration of smaller raindrops is prevalent during convective rain. Interestingly, convective rain over Rampurhat is associated with a higher concentration of both smaller and larger drops.

4.2 | GPM-DPR DSD observation

We also analyzed GPM-DPR-estimated D_m over both the locations. This analysis aims to investigate the variability of D_m across rainfall types, seasons, and regions, while validating the reliability of the results through interinstrumental comparisons between GPM-DPR and OPD

observations. This ensures the robustness and reliability of the analysis in understanding precipitation microphysics. The box plots of GPM-DPR-estimated D_m at Kohima and Rampurhat for stratiform and convective rain during the pre-monsoon and monsoon seasons are shown in Figure 5a,b, respectively. The corresponding values of the Q_2, Q_3, and UW values of the D_m parameter are provided in Table 3. The analysis of D_m values highlights significant seasonal, regional, and rain-type-specific variations. Seasonally, both Kohima and Rampurhat exhibit larger Q_2, Q_3, and UW values during the pre-monsoon compared to the monsoon season, indicating the presence of larger raindrop sizes in the pre-monsoon period, likely due to stronger convective activity. Regionally, Rampurhat consistently shows higher D_m values than Kohima for both stratiform and convective rain in both seasons, suggesting microphysical differences influenced by local atmospheric dynamics and topography. Convective rain demonstrates notably larger D_m values compared to stratiform rain at both stations and in both seasons, reflecting the role of intense updrafts in promoting the growth of larger raindrops. The largest D_m values are observed for convective rain at Rampurhat during the pre-monsoon, with a Q_3 of 2.4 mm and a UW of 4.0 mm, whereas the smallest D_m values occur for stratiform rain at Kohima during the monsoon, with a Q_2 of 1.0 mm and a UW of 1.6 mm. These findings emphasize the combined influence of regional, seasonal, and rain-type dynamics on raindrop size distributions. Overall, the results suggest that seasonally over each station and each type of rain, D_m is larger during the pre-monsoon compared to the monsoon season. Regionally, in each season and for each type of rain, D_m is larger at Rampurhat compared to Kohima. Across both stations and seasons, D_m is larger during convective rain compared to stratiform rain. The seasonal and regional variations of D_m for different types of rainfall observed from OPD are in agreement with the GPM-DPR observations. This consistency between independent datasets strengthens the reliability of our findings.

4.3 | Maritime and continental rain DSD characteristics

A scatter plot between the median values of $\log_{10}N_w$ and D_m with interquartile range (IQR) for different types of

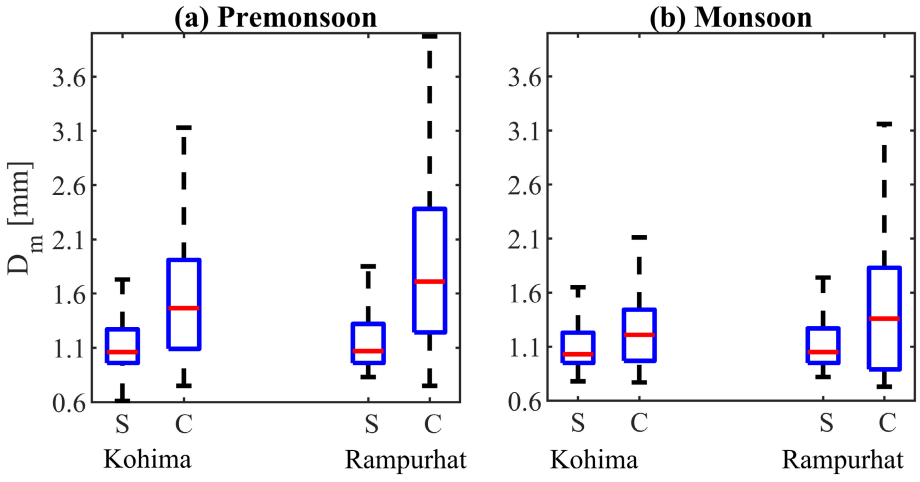

FIGURE 5 Box plots of GPM-DPR-derived D_m for stratiform (S) and convective (C) rain over Kohima and Rampurhat during the (a) pre-monsoon and (b) monsoon seasons. [Colour figure can be viewed at wileyonlinelibrary.com]

TABLE 3 D_m value for different types of rain at Kohima and Rampurhat during the pre-monsoon and monsoon seasons as observed from GPM-DPR measurements.

		D_m (mm)					
		Premonsoon			Monsoon		
Station		Q_2	Q_3	UW	Q_2	Q_3	UW
Kohima	Stratiform	1.1	1.3	1.7	1.0	1.2	1.6
	Convective	1.5	1.9	3.1	1.2	1.4	2.1
Rampurhat	Stratiform	1.1	1.3	1.9	1.1	1.3	1.7
	Convective	1.7	2.4	4.0	1.4	1.8	3.2

Abbreviations: Q_2, 50th percentile; Q_3, 75th percentile; UW, upper whisker.

rain during the pre-monsoon and monsoon seasons over Kohima and Rampurhat is shown in Figure 6 along with the maritime and continental regimes as suggested by Bringi et al. (2003). Two distinct clusters between $\log_{10}N_w$ and D_m are noted. The nature of the clusters suggests that the rain DSDs at Kohima exhibit maritime characteristics, while those at Rampurhat display continental characteristics during both seasons.

4.4 | Relationships of N_w–R and D_m–R

To facilitate the better parameterization of the normalized gamma rain DSD model over the study region, the power law relationships for N_w–R ($N_w = A_1R^{b1}$) and D_m–R ($D_m = A_2R^{b2}$) are derived. The occurrence of extremely intense rainfall ($R > 150\,\text{mm}\cdot\text{h}^{-1}$) at Rampurhat is noteworthy. The scatter plots of N_w–R at Kohima and Rampurhat for stratiform, mixed and convective types of rain during the pre-monsoon and monsoon seasons are shown in Figure 7. The values of coefficient A_1 are consistently higher during the monsoon compared to the pre-monsoon at both stations for all rain types, indicating a higher concentration of smaller raindrops in the monsoon.

Regionally, A_1 values were higher at Kohima than Rampurhat for all seasons and rain types, suggesting a greater concentration of smaller drops in Kohima.

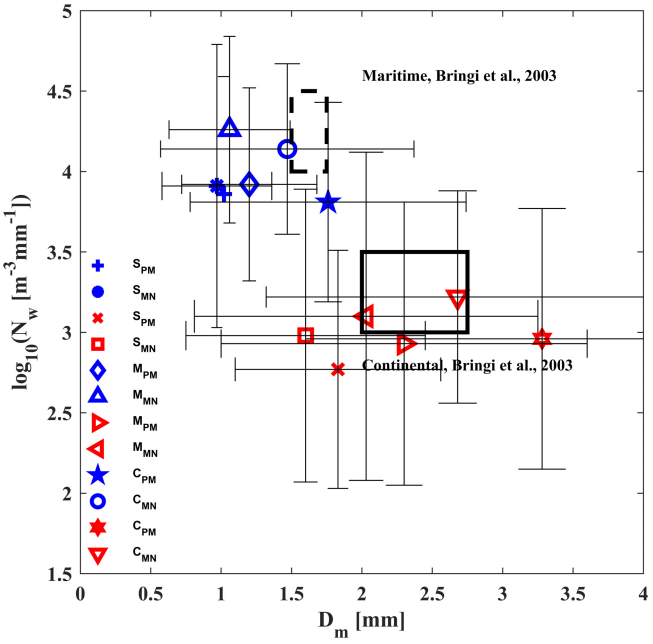

FIGURE 6 Scatter plot of the median values of $\log_{10}N_w$ versus D_m for different types of rain during the pre-monsoon and monsoon seasons over Kohima (blue) and Rampurhat (red). [Colour figure can be viewed at wileyonlinelibrary.com]

While stratiform rain generally exhibited lower A_1 values than convective rain, an exception occurred during the pre-monsoon at Rampurhat where stratiform rain had higher A_1 values.

Seasonally, exponent b_1 values are higher for all types of rain during the pre-monsoon in Rampurhat and during the monsoon in Kohima. Regionally, Rampurhat exhibits larger b_1 values across all rain types in the pre-monsoon, while in the monsoon, Kohima shows higher b_1 values, except for stratiform rain, where Rampurhat's values remain larger. In both seasons, stratiform rain over Rampurhat and convective rain over Kohima display large negative b_1 values, indicating a lower concentration of smaller drops with increasing R, suggesting dominant coalescence processes. Conversely, during the pre-monsoon in Rampurhat for convective rain, and during the monsoon in Kohima for stratiform rain, large positive b_1 values are observed, indicating a higher concentration of smaller drops with increasing R, likely due to increased drop breakup.

The scatter plots of D_m versus R at Kohima and Rampurhat for the stratiform, mixed and convective types of rain during the pre-monsoon and monsoon seasons are shown in Figure 8. The equation of the fitted power law ($D_m = A_2R^{b2}$) for each case is provided in the respective figure panels. The values of coefficient A_2 are consistently higher during the pre-monsoon compared to the monsoon at both stations for all rain types, indicating a predominance of larger raindrops in the pre-monsoon. Additionally, A_2 values were higher at Rampurhat than Kohima across all seasons and rain types, suggesting a greater prevalence of larger drops at Rampurhat. These regional and seasonal variations in coefficient A_2 are consistent with the corresponding patterns observed in D_m values. While stratiform rain generally exhibited higher coefficient values than convective rain, an exception occurred during the pre-monsoon at Rampurhat where convective rain had higher A_2 values.

Seasonally, values of exponent b_2 are higher for stratiform rain in the pre-monsoon and for the mixed and convective rain in the monsoon season over Rampurhat. In Kohima, larger b_2 values are observed for the stratiform and mixed rain in the pre-monsoon, and for convective rain in the monsoon season. Regionally, Rampurhat shows larger b_2 values for stratiform rain, while Kohima exhibits higher b_2 values for both mixed and convective rain in both seasons. In all cases, b_2 shows positive values indicating an increase in concentration of larger drops with increasing R, while stratiform rain over Rampurhat and convective rain over Kohima show larger b_2 values suggesting stronger drop coalescence.

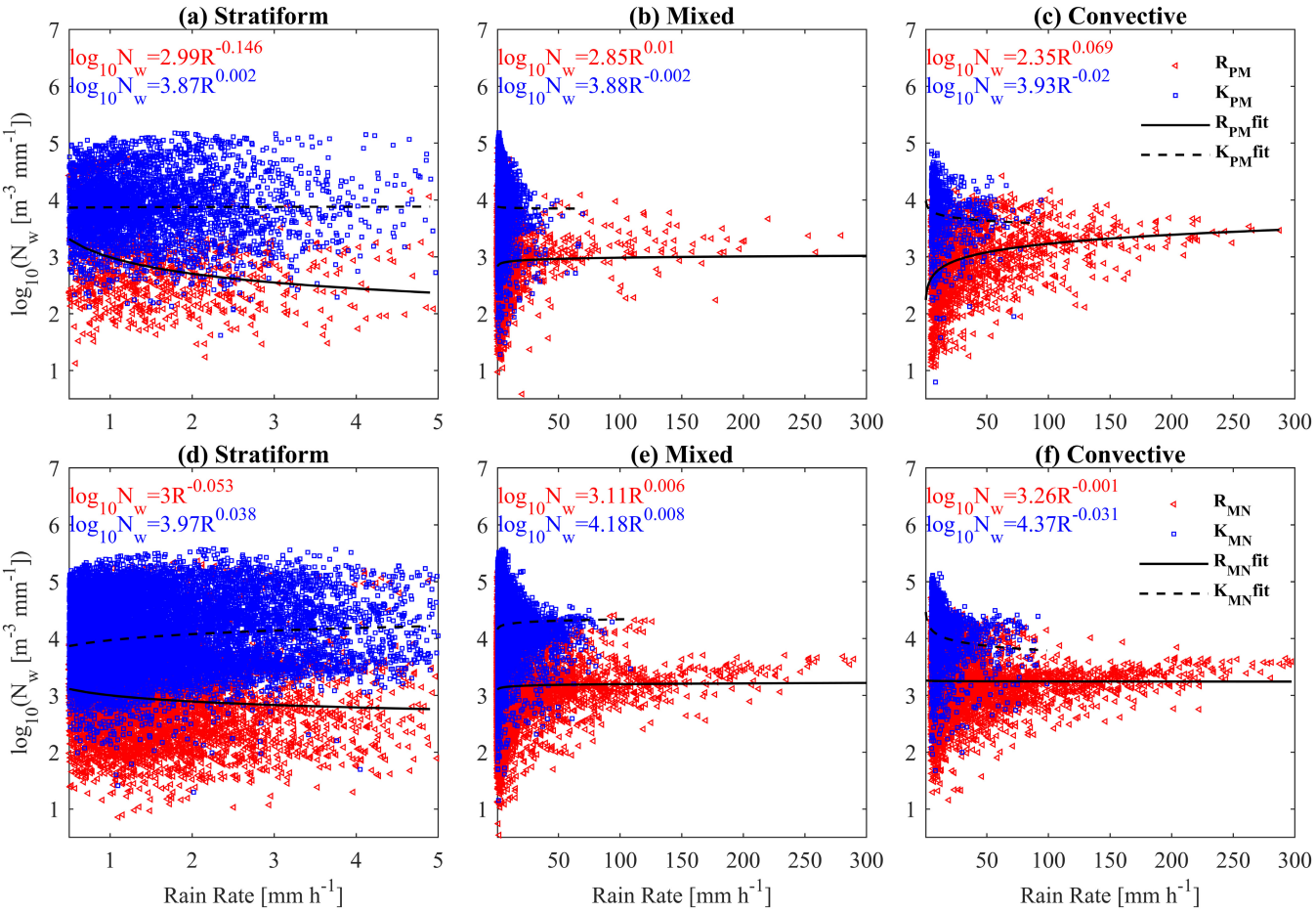

FIGURE 7 Scatter plot of N_w–R at Kohima (blue) and Rampurhat (red) for stratiform, mixed and convective rain during the pre-monsoon (upper panel) and monsoon (lower panel) seasons. [Colour figure can be viewed at wileyonlinelibrary.com]

4.5 | *Z–R* relationships and associated rain microphysical processes

To facilitate better estimation of rainfall from weather radar and to understand the involved microphysical processes for the observed rain DSD, the power law Z–R relationships are derived for each season at the two stations for different types of rain.

The scatter plots of Z versus R over Kohima and Rampurhat for stratiform, mixed and convective types of rain during the pre-monsoon and monsoon seasons are shown in Figure 9. The equation for the fitted power law ($Z = AR^b$) for each case is provided in the respective figure panels. Seasonally, it is found that, at both stations and for each type of rain, the coefficient value A is higher during the pre-monsoon season compared to the monsoon, suggesting the presence of larger drops during the pre-monsoon compared to the monsoon. Regionally, during both seasons, and for each type of rain the A value is higher at Rampurhat compared to Kohima, suggesting the presence of larger drops at Rampurhat compared to Kohima. In terms of rain type, except for the case of Rampurhat during the pre-monsoon season, the coefficient value is higher for stratiform rain compared to convective rain, whereas during the pre-monsoon at Rampurhat the coefficient value is higher for convective rain.

Overall, the seasonal and regional variation of the coefficient value of Z–R relations for each type of rain is consistent with the regional and seasonal characteristics of D_m–R relations. Similarly, the seasonal and regional variation of exponent b follows the same pattern with the seasonal and regional variation of the exponent b_2 of D_m–R relations.

Moreover, the value of exponent b of a Z–R relation provides information on the prevailing microphysical processes. In their study of the microphysical interpretation of the Z–R relation, Steiner et al. (2004) pointed out that the variability of the raindrop size distribution is bounded by either size- or number-controlled conditions, with conditions of a coordinated mixed control embedded in between those extremes. Based on raindrop spectra observations, Smith and Krajewski (1993) found the limiting values of the exponent b for number-controlled and size-controlled

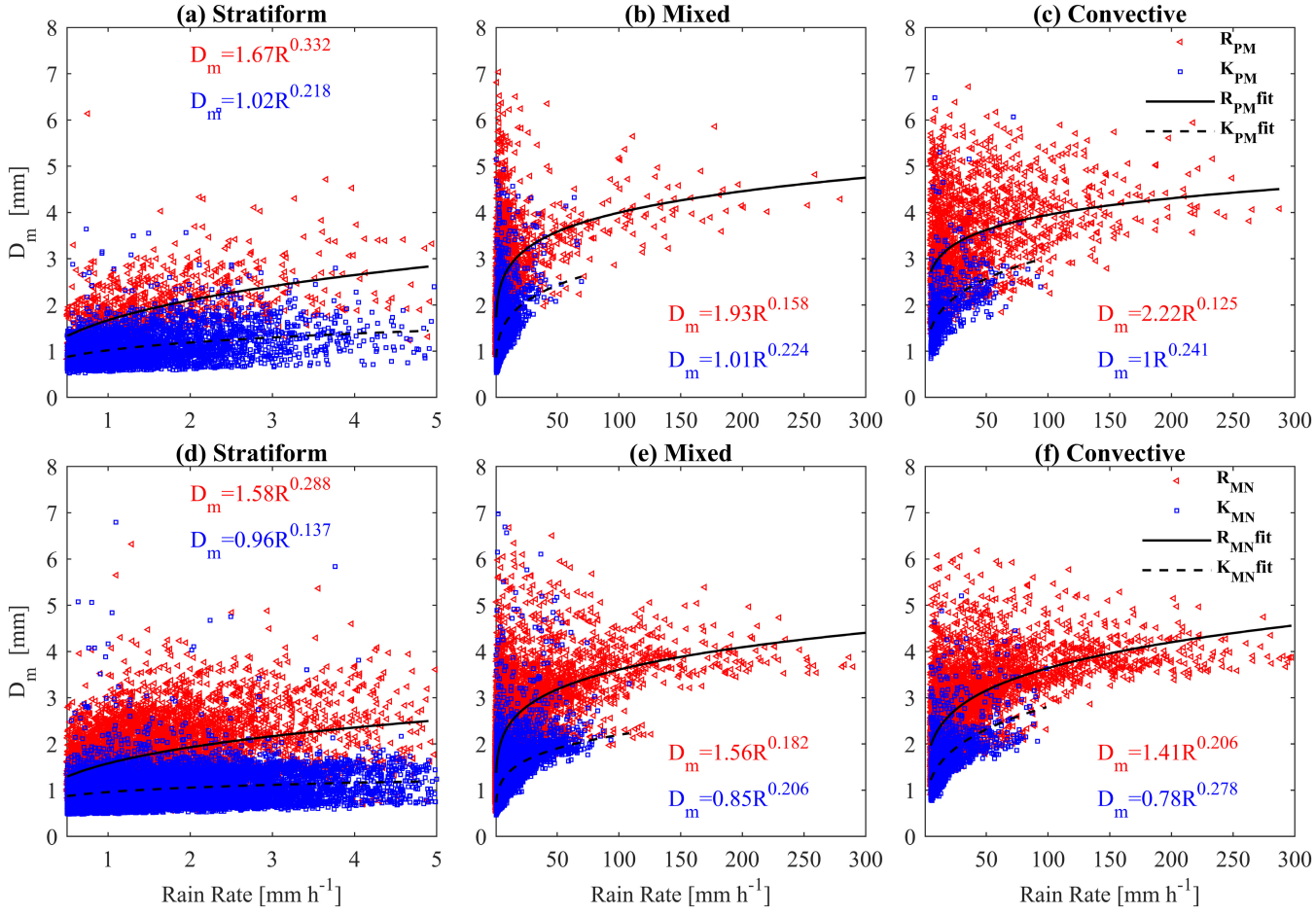

FIGURE 8 Scatter plots of D_m–R at Kohima (blue) and Rampurhat (red) for stratiform, mixed and convective rain during the pre-monsoon (upper panel) and monsoon (lower panel) seasons. [Colour figure can be viewed at wileyonlinelibrary.com]

conditions to be $1 \leq b < 1.79$. The lower value of b indicates the number-controlled process, whereas the higher value suggests the size-controlled process. Since convective, stratiform, and mixed categories have already been classified, it is easy to imagine that cloud microphysical processes will also differ according to each classification. In addition to this, the seasonal characteristics and differences between each of the locations examined in this study were also investigated.

During the pre-monsoon season at Rampurhat, stratiform rain is governed by the size-controlled process with a b value of 1.97, whereas mixed and convective rain are predominantly governed by coordinated mixed processes, with b values of 1.45 and 1.32, respectively. At Kohima, stratiform, mixed, and convective rain are governed by coordinated mixed processes with b values of 1.50, 1.51 and 1.66, respectively.

During the monsoon season at Rampurhat, stratiform rain is governed by the size-controlled process with a b value of 1.70, whereas mixed and convective rain are predominantly governed by the coordinated mixed process with b values of 1.48 and 1.52, respectively. At Kohima, stratiform and mixed rain are governed by the coordinated mixed process with b values of 1.32 and 1.44, respectively, while convective rain is found to be governed by the size-controlled process with a b value of 1.75. The results suggest a significant seasonal and regional variation in the prevailing microphysical processes, attributed to different climatic regimes.

To facilitate a comparative study with other stations across the globe, the coefficient A and exponent b of the Z–R relationship for different types of rain at various locations are presented in Table S2. The Z–R relationships obtained from OPD are included. Significant variations are observed in the coefficients and exponents of the Z–R relationships, highlighting substantial differences in the microphysical processes and properties from one location to another. Regardless of the rain type, the coefficients and exponents are found to range between 74 and 1408 and 1.22 and 1.97, respectively. This variation may be attributed to the different climatic regimes and prevailing microphysical processes. However, it is important to note

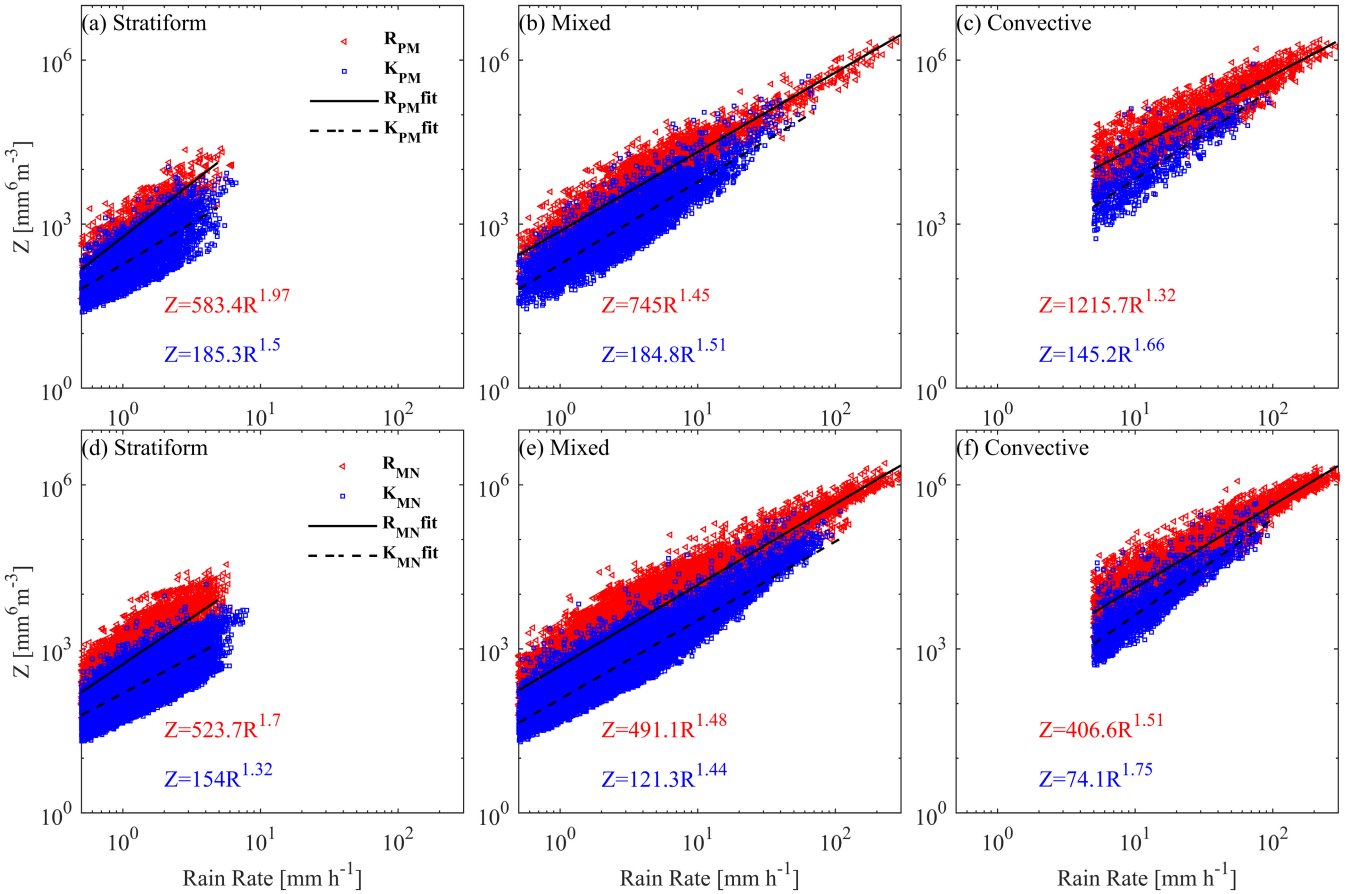

FIGURE 9 Scatter plots of Z–R at Kohima (blue) and Rampurhat (red) for the stratiform, mixed and convective rain during the pre-monsoon (upper panel) and monsoon (lower panel) seasons. [Colour figure can be viewed at wileyonlinelibrary.com]

that variations in Z–R relationships, in addition to being influenced by the type of rain, season, and geographical location, also depend on the measuring instruments, measurement techniques, sampling time, and analysis methods.

4.6 | Cloud Liquid Effective Radius profiles over Kohima and Rampurhat

The Cloud LER derived from the MODIS instrument onboard the Aqua satellite is used for understanding cloud and rain microphysics. LER provides insights into the size distribution of liquid cloud droplets, which plays a significant role in determining cloud optical properties, radiative behavior, and precipitation processes. In the context of cloud and rain microphysics, LER serves as a critical link between cloud microstructure and precipitation formation. Studies have demonstrated a relationship between droplet effective radius and precipitation water content, highlighting the importance of LER in understanding precipitation processes (Braga et al., 2021). Additionally, accurate retrievals of LER from satellite instruments like MODIS are essential for climate research, as they inform models that predict cloud behavior and precipitation patterns (Fu et al., 2022; Lin et al., 2023). Therefore, incorporating LER analysis into studies of cloud and rain microphysics enhances our comprehension of cloud development and precipitation mechanisms, contributing to improved weather forecasting and climate modeling. Box plots of Aqua-MODIS-derived LER during the pre-monsoon and monsoon seasons over Kohima and Rampurhat are shown in Figure 10a–d, respectively. During the pre-monsoon season the Q_2 (Q_3) values over Kohima and Rampurhat are found to be 14.5 μm (15.5 μm) and 16.0 μm (16.5 μm) respectively. Similarly, during the monsoon season they were found to be 10.5 μm (11.0 μm) and 13.0 μm (13.75 μm) over Kohima and Rampurhat, respectively.

It is observed that, seasonally, LER is larger during the pre-monsoon season compared to the monsoon season. During both seasons, LER is larger over Rampurhat than Kohima. The seasonal and regional variation of LER is consistent with the corresponding variation in D_m.

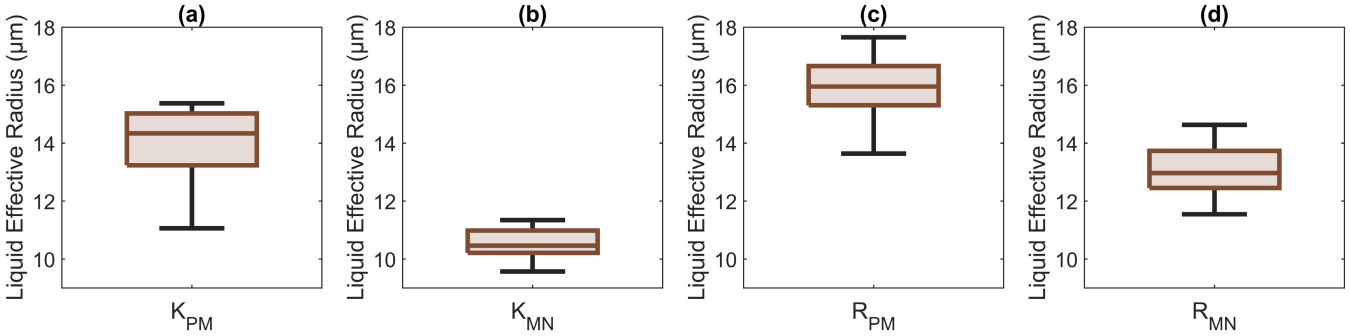

FIGURE 10 Box plots of cloud Liquid Effective Radius (LER) obtained from the Aqua-MODIS satellite over Kohima during the (a) pre-monsoon and (b) monsoon seasons, and over Rampurhat during the (c) pre-monsoon and (d) monsoon seasons. [Colour figure can be viewed at wileyonlinelibrary.com]

4.7 | Vertical velocity profiles over Kohima and Rampurhat

The height profiles of vertical velocities (ω, Pa·s^{-1}) are shown in Figure 11. The solid black line represents the mean value of ω at every vertical level. The horizontal error bars represent the standard deviations from the mean at each pressure level. Negative values indicate upward velocity and positive values indicate downward motion. At Kohima during the pre-monsoon and monsoon seasons, toward the lower heights (≤4.0 km) the mean value of ω is found to be approx. −0.05 and −0.04 Pa·s^{-1} respectively, whereas at Rampurhat, during the pre-monsoon and monsoon seasons, toward the lower heights (≤4.0 km) the mean ω is found to be approx. −0.11, and approx. −0.08 Pa·s^{-1}, respectively. At both stations, the standard deviation of ω during the pre-monsoon season is significantly higher compared to during the monsoon season. It is observed that seasonally, at both stations, ω is larger during the pre-monsoon than the monsoon season. Regionally, for each season, ω is larger at Rampurhat compared to Kohima. The results suggest a prevalence of stronger convection during the pre-monsoon season than the monsoon season. The seasonal and regional variation of ω is consistent with the rain drop size, which indicates that the occurrence of larger drops is associated with stronger convection.

5 | DISCUSSION AND SUMMARY

The seasonal and regional variation of surface DSDs was studied at Kohima in northeastern India and at Rampurhat in eastern India during the pre-monsoon and monsoon seasons. The rain DSDs are analyzed in terms of Λ, μ, N_w, D_m and Z. Seasonally, at both stations, both Λ and μ exhibit smaller values during the pre-monsoon season compared to the monsoon season. Regionally, Kohima shows larger values of both Λ and μ in both seasons compared to Rampurhat. Overall, convective rain exhibits lower Λ and μ values in both seasons at both stations compared to mixed and stratiform rain.

At both stations, the pre-monsoon season is found to be associated with smaller N_w and larger D_m compared to the monsoon season. Regionally, Kohima is associated with larger N_w and smaller D_m values compared to Rampurhat. Over Kohima stratiform rain shows a higher concentration of smaller drops whereas convective rain is associated with a higher concentration of larger drops.

However, at Rampurhat convective rain is associated with a higher concentration of both smaller and larger drops. The presence of large raindrops may be attributed to the strong in-cloud updraft which could suspend mid-size raindrops and help them collide and coalesce with other raindrops. Some of these raindrops can survive breakup processes and reach the surface while others can break up and further become smaller by evaporation. Note that smaller raindrops evaporate faster than big raindrops (Pruppacher and Klett, 1996). Another possible reason for the occurrence of smaller raindrops at Rampurhat could be the high cloud base and relatively drier atmosphere, which may cause additional evaporation and reduce raindrop size (see the Figure S2). Due to the above reasons, extremely small and large raindrops may occur over Rampurhat during convective rain. The D_m value from GPM-DPR was analyzed for variability across rainfall types, seasons, and regions to validate the reliability of the results through interinstrumental comparisons between GPM-DPR and OPD observations. The seasonal and regional variations of near-surface D_m for different types of rainfall, as observed from the GPM satellite's onboard Dual-frequency Precipitation Radar, are consistence with surface observations. The characteristics of the coefficient values in the N_w–R and D_m–R relationships for different

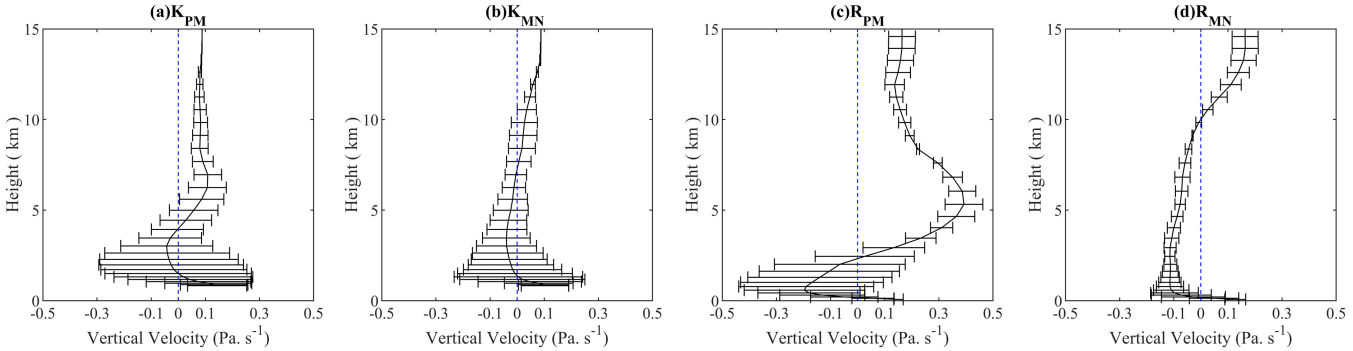

FIGURE 11 Height profiles of vertical velocity at Kohima during the (a) pre-monsoon and (b) monsoon seasons, and at Rampurhat during the (c) pre-monsoon and (d) monsoon seasons. [Colour figure can be viewed at wileyonlinelibrary.com]

types of rain are consistent with the regional and seasonal variations of N_w and D_m parameters, respectively. Overall, it is observed that, although both the stations are inland, the DSD characteristics at Kohima exhibit maritime features in both seasons, whereas those at Rampurhat exhibit continental characteristics. The maritime (continental) nature of rain DSDs at Kohima (Rampurhat) is primarily attributed to a shallow (deep) precipitating system over the northeastern (eastern) part of India (Roy et al., 2017).

The seasonal and regional variability of rain DSDs has also been reported by other researchers in different parts of India. Radhakrishna et al. (2009) found significant seasonal and regional differences in DSD between the inland station Gadanki in Andhra Pradesh and the coastal station Cuddalore in Tamil Nadu during the southwest and northeast monsoons. For the same R, the concentration of small drops is higher, while that of large drops is lower, during the northeast monsoon compared to the southwest monsoon at both locations. They also reported contrasting rain DSD characteristics at these two stations. Smaller and larger drops are found predominantly at Gadanki, whereas medium-sized drops are more prevalent at Cuddalore. The DSD differences are more pronounced during the northeast monsoon. They also noted that seasonal variation is less pronounced at Cuddalore compared to Gadanki. Over Gadanki, Reddy and Kozu (2003) and Rao et al. (2009) also reported larger rain drops during the southwest monsoon compared to the northeast monsoon. The seasonal variation of rain DSDs over the study region, showing larger drop sizes during the pre-monsoon compared to the monsoon season, is consistent with the findings of Kozu et al. (2006) and Sarma et al. (2016) at Gadanki as observed using a Joss Waldvogel Disdrometer, and of Longkumer et al. (2023) at Kohima, observed using a Micro Rain Radar (MRR). The larger raindrops during the pre-monsoon season are attributed to stronger vertical wind velocity driven by the atmospheric instability, lifting mechanism, and moisture availability over the region. The results from the present study show that DSDs are wider for convective rain and less spread out for stratiform rain, consistent with the results from Chen et al. (2013) and Zhang et al. (2019). Based on GPM-DPR observations, Radhakrishna et al. (2020) reported regional differences in rain DSDs across the Indian subcontinent and adjoining seas, with different topography, during the southwest monsoon. They reported significant differences in D_m values for a given R over land and sea, and orographic rain. Irrespective of R, the D_m values for deep rain were found to be larger in continental rain than in maritime and orographic rain. However, for shallow storms, the D_m values were smaller in continental rain than for orographic and maritime rain.

The scatter plot of D_m–$\log_{10}N_w$ shows two distinct clusters for Kohima and Rampurhat. At Kohima, it has lower D_m and higher $\log_{10}N_w$, whereas at Rampurhat, the opposite is observed with higher D_m and lower $\log_{10}N_w$. Overall, at Kohima (Rampurhat) the median values of D_m and lower N_w vary in the ranges of 1.0–1.8 mm (1.6–3.3 mm) and 3.8–4.3 (2.7–3.3), respectively. The D_m–$\log_{10}N_w$ values at Kohima, despite being an inland station, suggest a maritime characteristic, and the values at Rampurhat indicate a continental characteristic. This result is consistent with the reported maritime and continental rain DSD characteristics at various locations across the globe (Bringi et al., 2003; Radhakrishna et al., 2009; Shaik et al., 2024).

Broadly, the nature of the empirical relationships $\log_{10}N_w$–R derived at Kohima and Rampurhat during the monsoon seasons, where the coefficient values are found to be larger for convective rain compared to stratiform rain, is similar to those reported by Zhang et al. (2019) in southern China ($N_w = 11140R^{0.28}$ for convective rain; $N_w = 8920R^{0.28}$ for stratiform rain). Similarly, the nature of the empirical relationships D_m–R derived at Kohima and Rampurhat during the same seasons, where the coefficient values are found to be larger for stratiform rain compared to convective rain, is similar to the findings reported by Zhang et al. (2019) in southern China ($D_m = 1.4R^{0.14}$ for

convective rain; $D_m = 1.43R^{0.16}$ for stratiform rain). The smaller multiplicative coefficient value of the Z–R relationship at Kohima compared to Rampurhat is also in agreement with the maritime characteristics reported by Bringi et al. (2003).

Similarly, the regional and seasonal characteristics of the coefficient values of Z–R relationships for each type of rain are consistent with D_m variation. The value of exponent b of the Z–R relationships suggest that, during both seasons and at both stations, the microphysical processes are predominantly governed by coordinated mixed processes (i.e., number- and size-controlled processes), except for stratiform rain at Rampurhat during the pre-monsoon and monsoon seasons, and convective rain at Kohima, which are associated with size-controlled processes. The seasonal and regional variability of Z–R relationships has been extensively reported by many researchers worldwide, as shown in Table S2 (derived from the OPD). A wide variation in the A and b values is observed across the globe, which may be attributed to different climatic regimes and prevailing microphysical processes.

To understand cloud microphysical properties related to observed rain DSDs, Aqua-MODIS-measured cloud LER is considered. Seasonally, cloud LER is found to be larger during the pre-monsoon seasons compared to monsoon season. Regionally for each season, cloud LER is found to be larger over Rampurhat compared to Kohima. The seasonal and regional variation of reported cloud LER over the region is consistent with the reported seasonal and regional variation of cloud Ice Effective Radius (IER) (Biswasharma et al., 2021; Choudhury et al., 2015). The larger cloud LER and IER during the pre-monsoon season, as well as over eastern India (Rampurhat) is attributed to stronger convection, due to the higher magnitude of vertical velocity during the pre-monsoon season, as reported in the present work. Due to the larger value of Convective Available Potential Energy (CAPE) and the prevalence of colder clouds, stronger convection over Rampurhat compared to Kohima during the pre-monsoon season is also reported by Biswasharma et al. (2021). Similar results, that is, stronger convection over eastern India compared to the eastern Himalaya foothills, are also reported by Choudhury et al. (2015) and Roy et al. (2017, 2023). The shape of rain DSDs is significantly affected by the dynamical (Atlas et al., 2000; Kollias et al., 2001; Sharma et al., 2009) and microphysical processes (Sarma et al., 2016; Sharma et al., 2009; Ulbrich & Atlas, 2007). The presence of strong updrafts enhances the collision–coalescence process below freezing level and the rimming process above freezing level, which in turn results in the formation of larger raindrops which is reflected in larger value of D_m. The results of seasonal and regional variation of ω obtained from the ERA-5 dataset suggest the prevalence of stronger convection during the pre-monsoon compared to the monsoon season over both stations. The seasonal and regional variation of the nature of raindrop size is consistent with the nature of LER and ω, which suggests that the occurrence of larger drops during the pre-monsoon is associated with stronger convection in the season. The analysis of the Z–R relationship, cloud droplet size, and the vertical distribution of ω (Figures 9–11) highlights the physical processes that shape rain characteristics over Kohima and Rampurhat. Seasonal and regional differences in raindrop size are linked to the intensity of convection and cloud properties, particularly during the pre-monsoon season. Stronger updrafts during this period drive processes such as collision and coalescence of droplets, as evidenced by the larger cloud LER. This results in the formation of larger raindrops, further indicated by the higher coefficient of the Z–R relationship during the pre-monsoon compared to the monsoon season. These findings deepen our understanding of rainfall formation across different climatic regions and demonstrate how Z–R relationships are shaped by varying microphysical and dynamical conditions. In numerical modeling, this knowledge is essential for refining the parameterization of cloud microphysical processes, particularly in regions with strong seasonal variability. Improved representation of convective intensity and DSDs in models could enhance the accuracy of simulations for precipitation events. For weather forecasting, the observed seasonal variations in Z–R relationships provide a foundation for improving radar-based rainfall estimation techniques. Incorporating these findings into forecasting systems can enhance the reliability of real-time rainfall predictions and support early warning systems.

6 | CONCLUSIONS

A study on the seasonal and regional variation of rain DSDs, their properties, and associated microphysical processes for different rain types was conducted during the pre-monsoon and monsoon seasons at Kohima (northeast India) and Rampurhat (eastern India) using OPD observations. Rain is classified as stratiform, mixed and convective (Bringi et al., 2003). This study examines the seasonal and regional variation in rain DSD using the gamma model parameters and the variation of rain DSD properties in terms of Λ, μ, N_w, D_m and Z parameters. The summary of the study is as follows:

- Over Kohima, a constant peak diameter of 0.56 mm in the DSDs is observed for all rain types in both seasons, with a significant increase in drop concentration around the peak diameter as season progresses from pre-monsoon to monsoon. In contrast, at Rampurhat,

the peak diameter varies with both season and rain type, shifting toward smaller drops from pre-monsoon to monsoon.

- Rampurhat shows a predominance of larger drops ($D > 3$ mm) while Kohima shows a predominance of smaller drops ($D < 1$ mm) for all rain types in both seasons. Rampurhat has larger (smaller) values of D_m (Λ, μ, and N_w) compared to Kohima, indicating a higher concentration of larger raindrops and a lower concentration of smaller drops. The presence of extremely large raindrops (~8 mm) and intense rainfall ($R > 150$ mm·hr^{-1}) during convective rain can be noted.
- Convective rain shows larger (smaller) values of D_m (Λ, and μ) compared to stratiform rain in both regions, suggesting a higher concentration of larger raindrops during convective rain.
- Kohima has a higher concentration of smaller raindrops (larger $\log_{10}N_w$) during stratiform rain, while Rampurhat shows smaller drops alongside larger drops during convective rain.
- The pre-monsoon season shows a dominance of larger drops, while the monsoon season is characterized by smaller drops over both stations.
- During the pre-monsoon, larger values of D_m and smaller values of Λ, μ, and N_w are observed for all rain types at both stations, suggesting a higher concentration of larger raindrops and a lower concentration of smaller drops during the pre-monsoon.
- The seasonal variation of D_m for different types of rainfall, as observed from OPD, is consistent with the GPM-DPR observations.
- The scatterplot of D_m–$\log_{10}N_w$ shows the existence of two distinct clusters for Kohima and Rampurhat. The median values of D_m and N_w at Kohima (Rampurhat) range from 1.00–1.80 mm (1.60–3.30 mm) and 3.80–4.30 (2.70–3.30), respectively. The D_m–$\log_{10}N_w$ values at Kohima suggest a maritime characteristic, and those at Rampurhat suggest continental characteristics.
- Coefficients of N_w–R (D_m–R and Z–R) are larger during the monsoon (pre-monsoon) at both stations, indicating a higher concentration of smaller (larger) drops in the monsoon (pre-monsoon), respectively.
- Regionally, larger coefficient values of N_w–R (D_m–R and Z–R) are observed over Kohima (Rampurhat) during both seasons, with smaller (larger) drops over Kohima (Rampurhat). Stratiform rain shows smaller (larger) coefficient values at both stations, except during the pre-monsoon at Rampurhat, where convective rain shows smaller (larger) values. The exponent values of Z–R relationships indicate that microphysical processes are mainly governed by a coordinated mix process, except for stratiform rain at Rampurhat and convective rain at Kohima, which are associated with size-controlled processes.
- Cloud LER is larger in the pre-monsoon compared to the monsoon season at both stations, with larger values over Rampurhat than Kohima. This pattern is consistent with the variation in D_m.
- The seasonal and regional analysis of vertical velocity (ω) shows that negative ω values (upward motion) are larger in the pre-monsoon at Rampurhat. It suggests stronger convection and larger rain drops during the pre-monsoon at Rampurhat.

Overall, the present study demonstrates distinct seasonal and regional variability in rain DSDs and their associated microphysical processes for different types of rain over the eastern and northeastern parts of India. The study will help improve rainfall measurements through remote-sensing techniques in the region and contribute to better parameterization of rain processes in NWP models.

ACKNOWLEDGEMENTS

Financial support by the Ministry of Education, Govt of India, and Department of Higher Education, Nagaland, under the *Rashtriya Uchchatar Shiksha Abhiyan* (National Higher Education Mission) to carry out the present work is thankfully acknowledged. A research fellowship for Imolemba Longkumer is supported by the Council of Scientific and Industrial Research (CSIR), Govt. of India. The authors are thankful to the authority of Kohima Science College, Rampurhat College and Dimapur Government College for providing necessary facilities and support. Rupraj Biswasharma acknowledges the financial support from the Science and Engineering Research Board (SERB), Government of India, under NPDF (PDF/2022/002060). Imolemba Longkumer and Mahen Konwar thank IITM and MoES for the research facilities provided. We sincerely thank the editor and the two anonymous reviewers for their insightful comments on the manuscript, which helped improve its quality.

FUNDING INFORMATION

Financial support by the Ministry of Education, Govt of India, Department of Higher Education, Nagaland, under the *Rashtriya Uchchatar Shiksha Abhiyan* (National Higher Education Mission) to carry out the present work is thankfully acknowledged. A research fellowship for Imolemba Longkumer is supported by the Council of Scientific and Industrial Research (CSIR), Govt. of India. Rupraj Biswasharma acknowledges the financial support

from the Science and Engineering Research Board (SERB), Government of India, under NPDF (PDF/2022/002060).

CONFLICT OF INTEREST STATEMENT

The authors declare there are no conflicts of interest.

DATA AVAILABILITY STATEMENT

The data that support the findings of this study are available from the corresponding author upon reasonable request.

ORCID

Imolemba Longkumer https://orcid.org/0000-0002-0574-272X
Rupraj Biswasharma https://orcid.org/0000-0003-2582-7103
Mahen Konwar https://orcid.org/0000-0001-7489-5394

REFERENCES

Alhilali, M., Yin, I.H. & Din, J. (2018) Comparison of rain drop size distributions characteristics across the Southeast Asia region. *Telkomnika (Telecommunication Computing Electronics and Control)*, 16(6), 2522–2527.

Andsager, K., Beard, K.V. & Laird, N.F. (1999) Laboratory measurements of axis ratios for large raindrops. *Atmospheric Science*, 56, 2673–2683. Available from: https://doi.org/10.1175/1520-0469(1999)056%3C2673:LMOARF%3E2.0.CO;2

Atlas, D., Rosenfield, D., Short, D., Black, R.A., Amitai, E. & Willis, P.T. (2000) Partitioning tropical oceanic convective and stratiform rain by draft strength. *Journal of Geophysical Research: Atmospheres*, 105, 2259–2267.

Battaglia, A., Rustemeier, E., Tokay, A., Blahak, U. & Simmer, C. (2010) PARSIVEL snow observations: a critical assessment. *Journal of Atmospheric and Oceanic Technology*, 27, 333–344.

Bhatt, B.C. & Nakamura, K. (2005) Characteristics of monsoon rainfall around the Himalayas as revealed by TRMM precipitation radar. *Monthly Weather Review*, 133, 149–165.

Bhatt, B.C. & Nakamura, K. (2006) A climatological–dynamical analysis associated with precipitation around the southern part of the Himalayas. *Journal of Geophysical Research*, 111, D02115. Available from: https://doi.org/10.1029/2005JD006197

Biswasharma, R., Roy, P., Imolemba, Imlisunup, Samanta, D., Pramanik, G.P. et al. (2021) Regional variation of electrical and lightning properties of thunderclouds during the pre-monsoon season over the north-eastern and eastern part of India. *Atmospheric Research*, 260, 105683. Available from: https://doi.org/10.1016/j.atmosres.2021.105683

Braga, R.C., Rosenfeld, D., Krüger, O.O., Ervens, B., Holanda, B.A., Wendisch, M. et al. (2021) Linear relationship between effective radius and precipitation water content near the top of convective clouds: measurement results from ACRIDICON–CHUVA campaign. *Atmospheric Chemistry and Physics*, 21, 14079–14088. Available from: https://doi.org/10.5194/acp-21-14079-2021

Bringi, V.N., Chandrasekar, V., Hubbert, J., Gorgucci, E., Randeu, W.L. & Schoenhuber, M. (2003) Raindrop size distribution in different climatic regimes from disdrometer and dual-polarized radar analysis. *Journal of the Atmospheric Sciences*, 60, 354–365.

Chen, B., Yang, J. & Pu, J. (2013) Statistical characteristics of raindrop size distribution in the Meiyu season observed in eastern China. *Journal of the Meteorological Society of Japan. Ser. II*, 91(2), 215–227. Available from: https://doi.org/10.2151/jmsj.2013-208

Choudhury, H., Roy, P., Kalita, S. & Sharma, S. (2015) Spatio-temporal variability of the properties of mesoscale convective systems over a complex terrain as observed by TRMM sensors. *International Journal of Climatology*, 36, 2615–2632. Available from: https://doi.org/10.1002/joc.4516

Das, S.K., Konwar, M., Chakravarty, K. & Deshpande, S.M. (2017) Raindrop size distribution of different cloud types over the Western Ghats using simultaneous measurements from micro-rain radar and disdrometer. *Atmospheric Research*, 186, 72–82. Available from: https://doi.org/10.1016/j.atmosres.2016.11.003

Friedrich, K. & Kalina, E.A. (2013) Drop size distribution in thunderstorms measured by optical disdrometers during VORTEX2. *Monthly Weather Review*, 141, 1182–1203. Available from: https://doi.org/10.1175/MWR-D-12-00116.1

Friedrich, K., Higgins, S., Masters, F.J. & Lopez, C.R. (2013) Articulating and stationary PARSIVEL disdrometer measurements in conditions with strong winds and heavy rainfall. *Journal of Atmospheric and Oceanic Technology*, 30(9), 2063–2080. Available from: https://doi.org/10.1175/JTECH-D-12-00254.1

Friedrich, K., Kalina, E.A., Aikins, J., Steiner, M., Gochis, D., Kucera, P.A. et al. (2016) Rain drop size distributions and rain characteristics during the 2013 great Colorado flood. *Journal of Hydrometeorology*, 17(1), 53–72.

Fu, D., Di Girolamo, L., Rauber, R.M., McFarquhar, G.M., Nesbitt, S.W., Loveridge, J. et al. (2022) An evaluation of the liquid cloud droplet effective radius derived from MODIS, airborne remote sensing, and in situ measurements from CAMP2Ex. *Atmospheric Chemistry and Physics*, 22, 8259–8285. Available from: https://doi.org/10.5194/acp-22-8259-2022

Gatlin, P.N., Thurai, M., Bringi, V.N., Petersen, W., Wolff, D., Tokay, A. et al. (2015) Searching for large raindrops: a global summary of two-dimensional video disdrometer observations. *Journal of Applied Meteorology and Climatology*, 54, 1069–1089.

Goswami, B.B., Mukhopadhyay, P., Mahanta, R. & Goswami, B.N. (2010) Multiscale interaction with topography and extreme rainfall events in northeast Indian region. *Journal of Geophysical Research*, 115, D12114. Available from: https://doi.org/10.1029/2009JD012275

Hersbach, H., Bell, B., Berrisford, P., Biavati, G., Hor'anyi, A., Mu∼noz Sabater, J. et al. (2018) ERA5 hourly data on pressure levels from 1979 to present [data Set]. *Copernicus Climate Change Service (C3S) Climate Data Store (CDS)*. Available from: https://doi.org/10.24381/cds.bd0915c6

Hobbs, P.V. & Rangno, A.L. (2004) Super-large raindrops. *Geophysical Research Letters*, 31, L13102. Available from: https://doi.org/10.1029/2004GL020167

Houze, R.A., Wilton, D.C. & Smull, B.F. (2007) Monsoon convection in the Himalayan region as seen by the TRMM precipitation radar. *Quarterly Journal of the Royal Meteorological Society*, 133, 1389–1411.

Iguchi, T., Seto, S., Meneghini, R., Yoshida, N., Awaka, J. & Le, M. (2010) GPM/DPR level 2 algorithm theoretical basis docu-

ment, Technical Report. https://gpm.nasa.gov/sites/default/files/document_files/ATBD_DPR_201811_with_Appendix3b_0.pdf

Illiyas, F.T., Mohan, K., Mani, S.K. & Pradeepkumar, A.P. (2014) Lightning risk in India: challenges in disaster compensation. *Economic and Political Weekly*, 49(23), 23–27.

Jaffrain, J. & Berne, A. (2011) Experimental quantification of the sampling uncertainty associated with measurements from PARSIVEL disdrometers. *Journal of Hydrometeorology*, 12(3), 352–370. Available from: https://doi.org/10.1175/2010JHM1244.1

Janapati, J., Reddy, V., Reddy, K., Lin, P.L. & Liu, C.Y. (2017) A study on raindrop size distribution variability in before and after landfall precipitations of tropical cyclones observed over southern India. *Journal of Atmospheric and Solar-Terrestrial Physics*, 159, 23–40. Available from: https://doi.org/10.1016/j.jastp.2017.04.011

Ji, L., Chen, H., Li, L., Chen, B., Xiao, X., Chen, M. et al. (2019) Raindrop size distributions and rain characteristics observed by a PARSIVEL disdrometer in Beijing, Northern China. *Remote Sensing*, 11(12), 1479. Available from: https://doi.org/10.3390/rs11121479

Kollias, P., Albrecht, B.A. & Marks, F.D., Jr. (2001) Raindrop sorting induced by vertical drafts in convective clouds. *Geophysical Research Letters*, 28, 2787–2790. Available from: https://doi.org/10.1029/2.001GL013131

Konwar, M., Das, S.K., Deshpande, S.M., Chakravarty, K. & Goswami, B.N. (2014) Microphysics of clouds and rain over the Western Ghat. *Journal of Geophysical Research – Atmospheres*, 119, 6140–6159. Available from: https://doi.org/10.1002/2014JD021606

Konwar, M., Raut, B.A., Rao, Y.J. & Prabhakaran, T. (2022) Rain microphysical properties over the rain shadow region of India. *Atmospheric Research*, 275, 106224.

Kozu, T., Reddy, K.K., Mori, S., Thurai, M., Ong, J.T., Rao, D.N. et al. (2006) Seasonal and diurnal variation of rain drops size distribution in Asian monsoon region. *Journal of the Meteorological Society of Japan*, 84A, 195–209.

Krajewski, W.F., Anton, K., Clelia, C., Peter, G., Laurent, B., Jean-Dominique, C. et al. (2006) DEVEX-disdrometerevaluation experiment: basic results and implications for hydrologic studies. *Journal of Advanced Water Research*, 29(2), 311–325Available from: https://doi.org/10.1016/j.advwatres.2005.03.018

Krishna, U.V.M., Das, S.K., Sulochana, E.G., Bhowmik, U., Deshpande, S.M. & Pandithurai, G. (2021) Statistical characteristics of raindrop size distribution over the Western Ghats of India: wet versus dry spells of the Indian summer monsoon. *Atmospheric Chemistry and Physics*, 21, 4741–4757. Available from: https://doi.org/10.5194/acp-21-4741-2021

Kumar, S. & Silva, Y. (2019) Vertical characteristics of radar reflectivity and DSD parameters in intense convective clouds over south east South Asia during the Indian summer monsoon: GPM observations. *International Journal of Remote Sensing*, 40(24), 9604–9628. Available from: https://doi.org/10.1080/01431161.2019.1633705

Lavanya, S. & Kirankumar, N.V.P. (2021) Classification of tropical coastal precipitating cloud systems using disdrometer observations over Thumba, India. *Atmospheric Research*, 253, 105477.

Lin, K.-I., Chung, K.-S., Wang, S.-H., Chen, L.-H., Liou, Y.-C., Lin, P.-L. et al. (2023) Evaluation of hygroscopic cloud seeding in warm-rain processes by a hybrid microphysics scheme using a weather research and forecasting (WRF) model: a real case study. *Atmospheric Chemistry and Physics*, 23, 10423–10438. Available from: https://doi.org/10.5194/acp-23-10423-2023

Litta, A.J., Mohanty, U.C., Das, S. & Mary Idicula, S. (2012) Numerical simulation of severe local storms over east India using WRF-NMM mesoscale model. *Atmospheric Research*, 116, 161–184. Available from: https://doi.org/10.1016/j.atmosres.2012.04.015

Löffler-Mang, M. & Joss, J. (2000) An optical disdrometer for measuring size and velocity of hydrometeors. *Journal of Atmospheric and Oceanic Technology*, 17(2), 130–139. Available from: https://doi.org/10.1175/1520-0426(2000)017%3C0130:AODFMS%3E2.0.CO;2

Loh, J., Lee, D.-I. & You, C.-H. (2019) Inter-comparison of DSDs between Jincheon and Miryang at South Korea. *Atmospheric Research*, 227, 52–65. Available from: https/doi.org/10.1016/j.atmosres.2019.04.031

Longkumer, I., Biswasharma, R., Pongener, I., Roy, P., Samanta, D., Konwar, M. et al. (2023) A study of rain drop size distributions and associated rain microphysical processes over a subtropical station in the Northeast India. *Journal of Atmospheric and Solar-Terrestrial Physics*, 247, 106073. Available from: https://doi.org/10.1016/j.jastp.2023.106073

Marzano, F.S., Cimini, D. & Montopoli, M. (2010) Investigating precipitation microphysics using ground-based microwave remote sensors and disdrometer data. *Atmospheric Research*, 97, 583–600.

Marzuki, M., Hashiguchi, H., Yamamoto, M.K., Mori, S. & Yamanaka, M.D. (2013) Regional variability of raindrop size distribution over Indonesia. *Annales de Geophysique*, 31, 1941–1948.

Murata, F., Terao, T., Chakravarty, K., Jones, H., Syiemlieh, L. & Cajee, L. (2020) Characteristics of orographic rain drop-size distribution at Cherrapunji, Northeast India. *Atmosphere*, 11, 777. Available from: https://doi.org/10.3390/atmos11080777

Niu, S., Jia, X., Sang, J., Liu, X., Lu, C. & Liu, Y. (2010) Distributions of raindrop sizes and fall velocities in a semiarid plateau climate: convective versus stratiform rains. *Journal of Applied Meteorology and Climatology*, 49(4), 632–645. Available from: https://doi.org/10.1175/2009JAMC2208.1

Radhakrishna, B., Rao, T.N., Rao, D.N., Rao, N.P., Nakamura, K. & Sharma, A.K. (2009) Spatial and seasonal variability of rain drop size distributions in southeast India. *Journal of Geophysical Research*, 114, D04203. Available from: https://doi.org/10.1029/2008JD011226

Radhakrishna, B., Saikranthi, K. & Rao, T.N. (2020) Regional differences in raindrop size distribution within Indian subcontinent and adjoining seas as inferred from global precipitation measurement dual-frequency precipitation radar. *Journal of the Meteorological Society of Japan. Series II*, 98(3), 573–584. Available from: https://doi.org/10.2151/jmsj.2020-030

Rao, T.N., Radhakrishnan, B., Nakamura, K. & Rao, N.P. (2009) Differences in rain drop size distribution from south west monsoon to north east monsoon at Gadanki. *Quarterly Journal of the Royal Meteorological Society*, 135, 1630–1637.

Raupach, T.H. & Berne, A. (2015) Correction of raindrop size distributions measured by Parsiveldisdrometers, using a two-dimensional video disdrometer as a reference. *Atmospheric Measurement Techniques*, 8(1), 343–365. Available from: https://doi.org/10.5194/amt-8-343-2015

Reddy, K.K. & Kozu, T. (2003) Measurement of rain drop size distribution over Gadanki during south –west and north – east

monsoon. *Indian Journal of Radio & Space Physics*, 32, 286–295.

Romatschke, U. & Houze, J.R. (2011) Characteristics of precipitating convective systems in the pre monsoon season of south Asia. *Journal of Hydrometeorology*, 12, 157–180.

Romatschke, U. & Houze, R., Jr. (2011) Characteristics of precipitating convective systems in the south Asian monsoon. *Journal of Hydrometeorology*, 12, 3–26. Available from: https://doi.org/10.1175/2010JHM1289.1

Romatschke, U., Medina, S. & Houze, R., Jr. (2010) Regional, seasonal and diurnal variation of extreme convection in the south Asian region. *Journal of Climate*, 23, 419–439.

Roy, P., Biswasharma, R., Deshamukhya, A. & Sharma, S. (2020) Spatial and seasonal variation of rainfall contribution by the height spectrum of precipitation systems and associated cloud bulk properties over the South Asia. *International Journal of Climatology*, 40, 3771–3791. Available from: https://doi.org/10.1002/joc.6427

Roy, P., Biswasharma, R., Deshamukhya, A., Sharma, S. & Gairola, R.M. (2017) A study of the spatio-temporal variability of the properties of intense precipitation features over the south Asian region: an integrated multisensor approach. *International Journal of Climatology*, 37(S1), 624–639. Available from: https://doi.org/10.1002/joc.5027

Roy, P., Rao, T.N., Biswasharma, R., Sharma, S. & Das, S. (2023) Space–time variation of large hail-producing mesoscale convective systems over a complex terrain of the Indian subcontinent as revealed by the integrated tropical rainfall measuring Mission and global precipitation measurement observations. *International Journal of Climatology*, 43(6), 3023–3039. Available from: https://doi.org/10.1002/joc.8015

Sarma, A.C., Deshamukhya, A., Rao, T.N. & Sharma, S. (2016) A study of raindrop size distribution during stratiform rain and development of its parameterization scheme in the framework of multi-parameter observations. *Meteorological Applications*, 23(2), 254–268. Available from: https://doi.org/10.1002/met.1551

Seela, B.K., Janpati, J., Lin, P.-L., Reddy, K.K., Shirooka, R. & Wang, P.K. (2017) A comparison study of summer season rain drops size distribution between Palau and Taiwan, two islands in western Pacific. *Journal of Geophysical Research. Atmospheres*, 122(21), 11787–11805.

Sekhon, R.S. & Srivastava, R.C. (1971) Doppler radar observations of drop-size distributions in a thunderstorm. *Journal of the Atmospheric Sciences*, 28(6), 983–994.

Seto, S., Shimozuma, T., Iguchi, T. & Kozu, T. (2016) *Spatial and temporal variations of mass weighted mean diameter estimated by GPM/DPR*. Beijing, China: Paper presented at 2016 IEEE Intl. Geoscience and Remote Sensing Symposium. Available from: https://doi.org/10.1109/IGARSS.2016.7730023

Shaik, D.S., Madineni, V.R., Subrahmanyam, K., Madhavan, B.L. & Kumar, K.K. (2024) Seasonal dependence of characteristics of rain drop size distribution over two different climatic zones of India. *Meteorology and Atmospheric Physics*, 136, 12. Available from: https://doi.org/10.1007/s00703-024-01012-4

Sharma, S., Konwar, M., Sarma, D.K., Reddy, K.M. & Jain, A.R. (2009) Characteristics of rain integral parameters during tropical convective, transition and stratiform rain at Gadanki and its application in rain retrieval. *Journal of Applied Meteorology and Climatology*, 48, 1245–1266.

Smith, J.A. & Krajewski, W.F. (1993) A modeling study of rainfall rate-reflectivity relationships. *Water Resources Research*, 29, 2505–2514.

Steiner, M., Smith, J.A. & Uijlenhoet, R. (2004) A microphysical interpretation of the radar reflectivity–rain rate relationship. *Journal of the Atmospheric Sciences*, 61, 1114–1131.

Suh, S.H., Kim, H.J., Lee, D.I. & Kim, T.H. (2021) Geographical characteristics of rain drop size distribution in the southern parts of South Korea. *Journal of Applied Meteorology and Climatology*, 60, 157–169. Available from: https://doi.org/10.1175/JAMC-D-20-0102.1

Sulochana, Y., Rao, T.N., Sunilkumar, K., Chandrika, P., Raman, M.R. & Rao, S.V.B. (2016) On the seasonal variability of raindrop size distribution and associated variations in reflectivity–Rainrate relations at Tirupati, a tropical station. *Journal of Atmospheric and Solar-Terrestrial Physics*, 147, 98–105. Available from: https://doi.org/10.1016/j.jastp.2016.07.011

Sumesh, R.K., Resmi, E.A., Unnikrishnan, C.K., Jash, D., Sreekanth, T.S., Resmi, M.M., et al. (2019) Microphysical aspects of tropical rainfall during Bright Band events at mid and high-altitude regions over Southern Western Ghats, India. *Atmospheric Research*, 227, 178–197. Available from: https://doi.org/10.1016/j.atmosres.2019.05.002

Tanaka, H.L. & Yatagai, A. (2000) Comparative study of vertical motions in the global atmosphere 448 evaluated by various kinematic schemes. *Journal of the Meteorological Society of Japan*, 78, 289–298.

Tapiador, F.J., Checa, R. & De Castro, M. (2010) An experiment to measure the spatial variability of rain drop size distribution using sixteen laser disdrometers. *Geophysical Research Letters*, 37, L16803. Available from: https://doi.org/10.1029/2010GL044120

Tenorio, R.S., da Silva, C., Moraes, M. & Sauvageot, H. (2012) Rain drops size distribution and radar parameters in coastal tropical rain systems of northeastern Brazil. *Journal of Applied Meteorology and Climatology*, 51, 1960–1970.

Testud, J., Oury, S., Amayenc, P. & Black, R.A. (2001) The concept of "normalized" distributions to describe raindrop spectra: a tool for cloud physics and cloud remote sensing. *Journal of Applied Meteorology*, 40, 1118–1140.

Tokay, A. & Short, D.A. (1996) Evidence from tropical rain drop spectra of the origin of the rain from strartiform versus convective clouds. *Journal of Applied Meteorology*, 35, 506–531.

Tokay, A., Peterson, W.A., Gatlin, P. & Wingo, M. (2013) Comparison of rain drop sizedistribution measurements by collocated disdrometers. *Journal of Atmospheric and Oceanic Technology*, 30(8), 1672–1690.

Tokay, A., Wolff, D.B. & Peterson, W.A. (2014) Evaluation of the new version of the laser optical disdrometer, OTT Parsivel. *Journal of Atmospheric and Oceanic Technology*, 31, 1276–1288. Available from: https://doi.org/10.1175/jtech-d-13-00174.1

Ulbrich, C.W. (1983) Natural variation in the analytical form of the rain drop size distribution. *Journal of Climate and Applied Meteorology*, 22, 1764–1775.

Ulbrich, C.W. & Atlas, D. (1984) Assessment of the contribution of differential polarization to improved rainfall measurements. *Radio Science*, 19(1), 49–57.

Ulbrich, C.W. & Atlas, D. (2007) Microphysics of raindrop size spectra: tropical continental and maritime storms. *Journal of Applied Meteorology and Climatology*, 46, 1777–1791.

Wang, Y., Zheng, J., Cheng, Z. & Wang, B. (2020) Characteristics of raindrop size distribution on the eastern slope of the Tibetan plateau in summer. *Atmosphere*, 11, 562. Available from: https://doi.org/10.3390/atmos11060562

Wen, G., Xiao, H., Yang, H., Bi, Y. & Xu, W. (2017) Characteristics of summer and winter precipitation over northern China. *Atmospheric Research*, 197, 390–406.

Willis, P.T. (1984) Functional fits to some observed drop size distributions and parameterization of rain. *Journal of Atmospheric Sciences*, 41(9), 1648–1661.

Xie, Z., Yang, H., Lv, H. & Hu, Q. (2020) Seasonal characteristics of disdrometer-observed raindrop size distributions and their applications on radar calibration and erosion mechanism in a semi-arid area of China. *Remote Sensing*, 12(2), 262. Available from: https://doi.org/10.3390/rs12020262

Yamaji, M., Takahashi, H.G., Kubota, T., Oki, R., Hamada, A. & Takayabu, Y.N. (2020) 4-year climatology of global drop size distribution and its seasonal variability observed by spaceborne dual-frequency precipitation radar. *Journal of the Meteorological Society of Japan Series II*, 98(4), 755–773. Available from: https://doi.org/10.2151/jmsj.2020-038

Yamane, Y. & Hayashi, T. (2006) Evaluation of environmental conditions for the formation of severe local storms across the Indian subcontinent. *Geophysical Research Letters*, 33(17), L17806. Available from: https://doi.org/10.1029/2006GL026823

Yuter, S.E., Kingsmill, D.E., Nance, L.B. & Löffler-Mang, M. (2006) Observations of precipitation size and fall speed characteristics within coexisting rain and wet snow. *Journal of Applied Meteorology and Climatology*, 45(10), 1450–1464. Available from: https://doi.org/10.1175/JAM2406.1

Zeng, Y., Yang, L., Zhang, Z., Tong, Z., Li, J., Liu, F. et al. (2020) Characteristics of clouds and raindrop size distribution in Xinjiang, using cloud radar datasets and a disdrometer. *Atmosphere*, 11(12), 1382. Available from: https://doi.org/10.3390/atmos11121382

Zhang, A., Hu, J., Chen, S., Hu, D., Liang, Z., Huang, C. et al. (2019) Statistical characteristics of raindrop size distribution in the monsoon season observed in southern China. *Remote Sensing*, 11(4), 432. Available from: https://doi.org/10.3390/rs11040432

Zipser, E.J., Cecil, D.J., Liu, C., Nesbitt, S.W. & Yorty, D.P. (2006) Where are the most intense thunderstorms on earth? *Bulletin of the American Meteorological Society*, 87, 1057–1071.

SUPPORTING INFORMATION

Additional supporting information can be found online in the Supporting Information section at the end of this article.

How to cite this article: Longkumer, I., Biswasharma, R., Pongener, I., Samanta, D., Konwar, M. & Sharma, S. (2025) Seasonal and regional variation in drop size distributions for different types of rain over northeastern and eastern parts of India. *Quarterly Journal of the Royal Meteorological Society*, 151:e4951. Available from: https://doi.org/10.1002/qj.4951